Correlating galaxy colour and halo concentration: A tunable Halo Model of galactic conformity

Aseem Paranjape[⋆][1,2], Katarina Kovač[†][2], William G. Hartley[‡][2] and Isha Pahwa[§][1,3]
[1] *Inter-University Centre for Astronomy and Astrophysics, Ganeshkhind, Post Bag 4, Pune 411007, India*
[2] *Institute for Astronomy, Department of Physics, ETH Zürich, Wolfgang-Pauli-Strasse 27, CH 8093, Switzerland*
[3] *Leibniz-Institut für Astrophysik Potsdam (AIP), An der Sternwarte 16, D-14482 Potsdam, Germany*

21 September 2015

ABSTRACT

We extend the Halo Occupation Distribution (HOD) framework to generate mock galaxy catalogs exhibiting varying levels of "galactic conformity", which has emerged as a potentially powerful probe of environmental effects in galaxy evolution. Our model correlates galaxy colours in a group with the concentration of the common parent dark halo through a "group quenching efficiency" ρ which makes older, more concentrated halos *at fixed mass* preferentially host redder galaxies. We find that, for a specific value of ρ, this 1-halo conformity matches corresponding measurements in a group catalog based on the Sloan Digital Sky Survey. Our mocks also display conformity at large separations from isolated objects, potentially an imprint of halo assembly bias. A detailed study – using mocks with assembly bias erased while keeping 1-halo conformity intact – reveals a rather nuanced situation, however. At separations $\lesssim$ 4Mpc, conformity is mainly a 1-halo effect dominated by the largest halos and is *not* a robust indicator of assembly bias. Only at very large separations ($\gtrsim$ 8Mpc) does genuine 2-halo conformity, driven by the assembly bias of small halos, manifest distinctly. We explain all these trends in standard Halo Model terms. Our model opens the door to parametrized HOD analyses that self-consistently account for galactic conformity at all scales.

Key words: galaxies: formation – cosmology: dark matter, large-scale structure of Universe – methods: N-body, numerical

1 INTRODUCTION

The processes that cause star formation activity in galaxies to diminish or "quench" are of great interest in understanding galaxy evolution. A number of observational and (semi-)numerical studies (van den Bosch et al. 2008; Ross & Brunner 2009; Wetzel & White 2010; van der Wel et al. 2010; Hopkins et al. 2010; More et al. 2011; Prescott et al. 2011; Wetzel et al. 2012, 2013; Cen 2014; Hirschmann et al. 2014) have attempted to distinguish between the relative importance of galaxy mergers (Toomre & Toomre 1972) and wider halo-level physical processes such as ram-pressure stripping of gas (Gunn & Gott 1972), "strangulation" (Larson et al. 1980; Balogh & Morris 2000), "harassment" (Moore et al. 1996), etc. that may lead to quenching in group environments (for a recent review, see Somerville & Davé 2014). Even where halo-level effects are indicated, there is ongoing debate over whether the location of a galaxy within its group (i.e. whether it is a "central" galaxy or a "satellite") is paramount (Baugh 2006; Peng et al. 2012;

Kovač et al. 2014), or whether the nature of the group as a whole is more important in quenching its member galaxies (Osmond & Ponman 2004; van den Bosch et al. 2008; Carollo et al. 2014; Hartley et al. 2015; Knobel et al. 2014).

In this context, a particularly interesting phenomenon that has received attention recently is that of "galactic conformity" (Weinmann et al. 2006). This is the observation that satellite galaxies in groups whose central galaxy is quenched (or red) are preferentially quenched, even when the groups are restricted to reside in dark matter halos of the same mass (see Knobel et al. 2014, for an in-depth study extending this statement to a variety of measures of environment). Weinmann et al. (2006) based these conclusions on a group catalog (Yang et al. 2005) constructed using galaxies in the Sloan Digital Sky Survey (SDSS). More recently, a similar effect has been observed by Kauffmann et al. (2013) when studying the star formation rates (SFR) of SDSS galaxies at large spatial separations ($\lesssim$ 4Mpc) from isolated objects.

The observation of galactic conformity contradicts an assumption typically made in halo occupation models of galaxy distributions, namely, that galaxy properties such as luminosity and colour distributions are determined solely by the mass of the parent dark halo of the group to which the galaxy belongs. Modelling conformity then becomes important in

⋆ Email: aseem@iucaa.ernet.in
† Email: kovac@phys.ethz.ch
‡ Email: hartleyw@phys.ethz.ch
§ Email: ipahwa@aip.de

order to better understand the galaxy-dark matter connection (Zentner et al. 2014), with consequences for both semi-analytical models of galaxy evolution (Wang et al. 2013; Kauffmann et al. 2013) as well as statistical studies aimed at constraining cosmological parameters (van den Bosch et al. 2013; More et al. 2015; Coupon et al. 2015).

It is tempting to ascribe a physical origin to galactic conformity, as Hartley et al. (2015) do. Since the seminal work of Fabian et al. (2003), evidence for regulation of the hot gas temperature in clusters of galaxies, by the super-massive black hole (SMBH) at the centre of the brightest cluster galaxy, has been growing (Croton et al. 2006; Zhuravleva et al. 2014). Although it is not clear whether a similar regulation exists for group-mass halos, a coupling of the star-formation properties of different group members via the hot gas content of their halo provides a natural explanation for conformity; a coupling that could even be established many Gyrs previously (Rawlings & Jarvis 2004). A coupling such as this may also exist due to re-processing of the gas content of individual galaxies in a group (Oppenheimer et al. 2010; Birrer et al. 2014). However, this is far from a unique solution. We might equally speculate that the virial shock heating of infalling gas depend on the halo's location within the cosmic web, perhaps being more effective in filaments than in voids at low halo masses for instance. In each of these hypothetical cases the conformity signal found by Weinmann et al. (2006) and others is driven by a hidden variable (past/present SMBH activity or large scale environment), i.e. a quantity that was not accounted for in those studies. Clearly identifying the correct hidden variable(s), those that "explain" conformity, will lead us to a greater understanding of the physical nature of quenching in galaxy groups.

An obvious suspect as to the hidden variable, and therefore the possible origin of galactic conformity, is the assembly history of the parent halo. The phenomenon of halo assembly bias, in which low mass older halos tend to cluster more strongly at scales $\gtrsim$ 10Mpc than younger, more recently assembled halos of the same mass (while this trend reverses for more massive halos) is well established (Sheth & Tormen 2004; Gao et al. 2005; Wechsler et al. 2006; Jing et al. 2007; Desjacques 2008; Dalal et al. 2008; Hahn et al. 2009; Fakhouri & Ma 2010). Halo age also correlates well with other halo properties – we will focus on halo concentration which correlates positively with age (Navarro et al. 1997; Wechsler et al. 2002) – and halo assembly bias has been observed to extend to these properties as well; e.g., at fixed low mass, more concentrated halos typically cluster more strongly than less concentrated ones.

Viewed from the present day, a halo that has a low late-time mass accretion (with respect to other similar mass haloes) would have a higher formation redshift and, statistically, a greater concentration. In relatively low-mass haloes the build up of dark matter mass and the accretion of baryons by the central galaxy are quite tightly coupled, because the time scale for cooling to offset gravitational heating is shorter than the free-fall time White & Rees (1978). The galaxies hosted by early-forming haloes would therefore experience a reduced supply of star-forming gas with respect to the larger galaxy population, and in the most extreme cases could result in a higher probability of being quenched. A plausible hypothesis, then, is that halo assembly bias affects galaxy formation and leads to a *galaxy* assembly bias (Tinker et al. 2012), which leaves an imprint in the form of galactic conformity (Hearin et al. 2015). More specifically, according to this hypothesis

galactic conformity both within individual groups *as well as* at large scales may be explained if, at fixed halo mass and galaxy luminosity/stellar mass, quenched or red galaxies preferentially reside in older (sub)halos.

One point of interest in this regard is that the conformity signal observed by Kauffmann et al. (2013) at scales $\lesssim$ 4Mpc is quite strong (roughly an order of magnitude difference in the median specific SFR of galaxies surrounding isolated objects that belong to the upper and lower 25th percentiles of specific SFR). Halo assembly bias, on the other hand, has been argued to be relatively unimportant in modelling, e.g., the dependence of galaxy 2-point correlation functions on properties such as luminosity, colour and SFR at similar scales (e.g., Skibba & Sheth 2009; Deason et al. 2013). It is therefore important to ask how assembly bias can be simultaneously consistent with these observations, or whether some other mechanism could generate the conformity signal.

In principle, such a test can be performed by embedding an assumed conformity-inducing correlation between galaxy and halo properties in an analytical Halo Model framework (for a review, see Cooray & Sheth 2002), since it is feasible to accurately model property-dependent clustering in this language (Wechsler et al. 2006). However, comparing analytical calculations directly with observations can become quite involved in the presence of possibly complex selection criteria used in defining the observed sample and the signal itself. A more efficient method, then, is to use N-body simulations of dark matter and construct mock galaxy catalogs in which one has full control over switching the conformity signal on and off; these mocks can then be analysed in the same way as the observed sample for a fair comparison. Such mock catalogs have recently been presented by Hearin & Watson (2013); Masaki et al. (2013b); Hearin et al. (2014a) who model galactic conformity by introducing a rank ordering of galaxy colours or SFR by suitably defined measures of (sub)halo age. The "age matching" mocks of Hearin & Watson (2013) and Hearin et al. (2014a) have been shown to successfully reproduce a number of observed trends such as the 2-point correlation function and galaxy-galaxy lensing signal of SDSS galaxies (Hearin et al. 2014b), the radial profile of the satellite quenched fraction in groups (Watson et al. 2015), etc., in addition to containing a conformity signal. The rank ordering in these mocks leads to a fixed strength of galactic conformity, however (see, e.g., Figure 3 in Hearin et al. 2015). In the absence of conclusive evidence as to the nature of the hidden variable that explains conformity, it is then interesting to explore alternative algorithms, particularly those that implement a *tunable* effect which can then be compared with observations.

Another relevant issue is that it is important to be able to distinguish cleanly between conformity within individual groups and conformity effects due to spatial correlations between distinct halos (these were respectively dubbed "1-halo" and "2-halo conformity" by Hearin et al. 2015). This is because the distinction between what is inside and outside a dark halo becomes fuzzy in any analysis that averages over a large range of halo masses. E.g., we would like to ask the following: out to what spatial separations might one see the effects of conformity in a model that has *only* 1-halo conformity built in and *does not* know about the large scale environmental correlations due to halo assembly bias? This might plausibly be the case in a halo-specific gas regulation mechanism that couples to star formation activity as mentioned above. This question is particularly interesting in the context of the apparent con-

flict in the expected strength of galaxy assembly bias and the observed strength of galactic conformity mentioned above.

In this paper we introduce an algorithm that allows us the level of control needed to address the above issues. Our algorithm is a modification and extension of the one described in Skibba & Sheth (2009, hereafter, S09) to model galaxy positions, luminosities and colours; we model galactic conformity by introducing a positive correlation between galaxy colour and the concentration of the parent dark halo *of the group* to which the galaxy belongs (i.e., we work at the level of groups and not subhalos). The strength of this correlation is determined by adjusting the value of a parameter ρ which we interpret as a "group quenching efficiency", the terminology being motivated by similar quantities studied by earlier authors (see, e.g., van den Bosch et al. 2008; Peng et al. 2010; Knobel et al. 2014). In order to answer the question regarding large scale effects raised above, we also explore a model where halo concentrations are *randomized* among halos of fixed mass before correlating them with the galaxy colours, thereby erasing any large scale clustering of the colours due to halo assembly bias while keeping average group-specific properties (including 1-halo conformity) intact.

The paper is organised as follows. In section 2 we describe the S09 algorithm, followed by our modifications for correlating galaxy colours with halo concentrations and calculating stellar masses. In section 3 we describe the N-body simulations on which our mock galaxy catalogs are based. Section 4 describes the SDSS-based group catalog that we use for comparison with our mocks, together with various fitting functions derived from this sample which inform our mocks. Our results are described in section 5, followed by a discussion in section 6. We conclude in section 7. We will use SDSS galaxy properties K-corrected to redshift $z = 0.1$, usually denoted by a superscript, e.g., $^{0.1}r$ for the r band. Throughout, we will denote $M_{0.1_r} - 5\log_{10}(h)$ as M_r, $^{0.1}(g - r)$ as $g - r$ and quote stellar masses $m_\star$ in units of $h^{-2}M_\odot$ and halo masses m in units of $h^{-1}M_\odot$, where $H_0 = 100\,h\,\mathrm{km\,s^{-1}Mpc^{-1}}$ is the Hubble constant. We use a flat ΛCDM cosmology with parameters $\Omega_\mathrm{m} = 0.25$, $\Omega_\mathrm{b} = 0.045$, $h = 0.7$, $\sigma_8 = 0.8$ and $n_\mathrm{s} = 0.96$, which are consistent with the 5-year results of the WMAP experiment (Hinshaw et al. 2009).

2 ALGORITHM

Our basic algorithm is borrowed from S09 and is itself an extension of the algorithm described by Skibba et al. (2006) to include galaxy colours. The algorithm uses a Halo Occupation Distribution function (HOD; Berlind & Weinberg 2002) calibrated on SDSS luminosity-dependent projected clustering measurements to create a luminosity-complete mock galaxy catalog. We describe this algorithm and our modifications below.

2.1 The S09 algorithm

2.1.1 Luminosities, positions and velocities of centrals and satellites

The S09 algorithm explicitly implements the so-called central-satellite split. A fraction $f_\mathrm{cen}(< M_{r,\mathrm{max}}|m)$ of m-halos (i.e., halos with masses in the range $(m, m + \mathrm{d}m)$) is chosen to have a central galaxy brighter than the luminosity threshold $M_{r,\mathrm{max}}$.

Each m-halo with a central is then assigned a number of satellites drawn from a Poisson distribution with mean $\bar{N}_\mathrm{sat}(< M_{r,\mathrm{max}}|m)$. The luminosities of centrals and satellites are then assigned using the distributions $f_\mathrm{cen}(< M_r|m)/f_\mathrm{cen}(< M_{r,\mathrm{max}}|m)$ and $\bar{N}_\mathrm{sat}(< M_r|m)/\bar{N}_\mathrm{sat}(< M_{r,\mathrm{max}}|m)$, respectively. The functions $f_\mathrm{cen}(< M_r|m)$ and $\bar{N}_\mathrm{sat}(< M_r|m)$ define the HOD, with the mean number of galaxies brighter than M_r residing in m-halos given by $\langle N_\mathrm{gal}|m \rangle = f_\mathrm{cen}(< M_r|m)\left[1 + \bar{N}_\mathrm{sat}(< M_r|m)\right]$. In this work we will use the forms calibrated by Zehavi et al. (2011); specifically, we use an interpolation kindly provided by Ramin Skibba. Our fiducial cosmology has the same parameter values as used by Zehavi et al. (2011) for their HOD analysis. Satellite luminosities are assigned after the central ones, and the algorithm ensures that the central is the brightest galaxy of the group. We will return to this point later.

Each central is placed at the center-of-mass of its parent dark matter halo and is assigned the velocity of the halo. The satellites are distributed around the centrals according to a truncated Navarro-Frenk-White (NFW) profile (Navarro et al. 1996), using a halo concentration as described below, and are assigned random velocities relative to the central that are drawn from a Maxwell-Boltzmann distribution that scales with halo mass[1]. This procedure for assigning satellite positions and velocities is more efficient, but perhaps less accurate, than identifying satellites with subhalo positions (e.g., there is no information regarding infall times and number of pericenter passages, but we need not run a very high resolution simulation and track low mass subhalos).

2.1.2 Galaxy colours and the central-satellite split

Having assigned galaxy positions, velocities and luminosities, galaxy colours are assigned by drawing from double-Gaussian fits to the observed distribution of $g - r$ colours at fixed luminosity. The two components of the double-Gaussian – 'red' and 'blue' – have means, variances and relative fraction as functions of luminosity that are fit to data. We give the results of such fits to SDSS data in section 4.3. Since these fits work at the level of the full galaxy sample, there is some freedom in deciding what fraction of centrals and satellites at fixed luminosity must be labelled 'red' with the above definition. This is a somewhat subtle issue which merits some discussion.

In general, one might assume that the central and satellite red fractions depend on both luminosity of the object as well as the mass of the parent halo, and we would denote these quantities as $p(\mathrm{red}|\mathrm{cen}, M_r, m)$ and $p(\mathrm{red}|\mathrm{sat}, M_r, m)$, respectively. S09 showed that a model in which these quantities do not depend on halo mass (but have a non-trivial luminosity dependence) is consistent with measurements of colour-marked clustering of SDSS galaxies. However, colour-dependent clustering measurements will also depend on the level of conformity, which is what we are trying to model here (and which S09 did not do). We therefore adopt a simpler approach: we continue to assume that these red fractions are independent of halo mass, but fix the form of $p(\mathrm{red}|\mathrm{sat}, M_r)$ by demanding agreement with a direct measurement of this quantity in an SDSS-based group catalog (Yang et al. 2007, henceforth,

---

[1] We note that our analysis in this paper does not use information regarding galaxy velocities; this will however be essential in future work when comparing, e.g., to observations of clustering in redshift space.

Y07). The form of $p(\mathrm{red}|\mathrm{cen}, M_r)$ is then fixed by the assumed HOD, while the *all*-galaxy red fraction $p(\mathrm{red}|M_r, m)$ inherits a mass dependence from the HOD (see Appendix A1)[2]. In Appendix A1 we also explore the consequences of a halo mass dependence in the red fraction of centrals.

The S09 algorithm has been used in several studies of galaxy environments (e.g., Muldrew et al. 2012; Skibba et al. 2013) and the luminosity and color dependence of galaxy clustering (e.g., Skibba et al. 2014; Carretero et al. 2015). We modify and extend this algorithm in two ways: (i) we correlate galaxy colours with the parent halo concentration and (ii) we calculate a stellar mass for each galaxy using a colour-dependent mass-to-light ratio.

2.2 Correlating colour and concentration

As indicated above, in the basic S09 algorithm the colour of any given galaxy is assigned in two steps: first the galaxy is labelled 'red' (a 'red flag' is set to 1) with probability $p(\mathrm{red}|\mathrm{gal}, M_r)$ where 'gal' is either 'cen' or 'sat', and then its colour is drawn as a Gaussian random number with the appropriate mean and variance. We correlate galaxy colours with parent halo concentrations by modifying the first step to adjust the red flag according to the concentration. The trend we wish to introduce is that more concentrated, older halos should host older, or redder, galaxies.

At fixed halo mass, halo concentration c is approximately Lognormally distributed, i.e. $\ln c$ is approximately Gaussian distributed with constant scatter $\sigma_{\ln c} \simeq 0.14 \ln(10)$ and a mean value $\langle \ln c \rangle \equiv \ln \bar{c}(m, z)$ that depends on halo mass and redshift (see, e.g. Bullock et al. 2001; Wechsler et al. 2002). In the range of interest the mean value is well described by (Ludlow et al. 2014)

$$\bar{c}(m, z) = \alpha \, \nu(m, z)^{-\beta}, \qquad (1)$$

where $\nu(m, z) = \delta_c(z)/\sigma(m)$ is the dimensionless "peak height" of the halo[3] and the coefficients α and β depend on the choice of halo mass definition. We will construct catalogs using the $m_{200\mathrm{b}}$ definition for which the Zehavi et al. (2011) HOD was calibrated ($m_{200\mathrm{b}}$ is the mass contained in the radius $R_{200\mathrm{b}}$ where the spherically averaged density is 200 times the background matter density $\bar{\rho}(z)$) and the corresponding $\bar{c}(m, z)$ relation. For this choice we have $\alpha = 7.7$ and $\beta = 0.4$ (see, e.g., Appendix A of Paranjape 2014).

Let $p(\mathrm{red})$ be the value of the red fraction in the *absence* of any correlation with concentration. (For clarity we drop the explicit dependence on galaxy luminosity and type.) It is useful to define the quantity

$$s \equiv \frac{\ln(c/\bar{c})}{\sigma_{\ln c}}, \qquad (2)$$

whose distribution $p(s)$ is Gaussian with zero mean and unit variance, with $\bar{c}(m)$ and $\sigma_{\ln c}$ defined above. We compute a conditional red fraction $p(\mathrm{red}|s)$ that depends on the parent halo concentration by setting

$$p(\mathrm{red}|s) = (1 - \rho)p(\mathrm{red}) + \rho \, \Theta(s - s_{\mathrm{red}}), \qquad (3)$$

where the Heaviside function $\Theta(x)$ is unity for $x > 0$ and zero otherwise. This says that galaxies in halos with concentrations $s > s_{\mathrm{red}}$ have an enhanced probability to be red as compared to the S09 model, while this probability is lowered by a factor $(1 - \rho)$ compared to $p(\mathrm{red})$ for galaxies in low-concentration halos. The dividing line s_{red} between high and low concentrations is defined in such a way that the *average* red fraction across all halos satisfies

$$\langle \, p(\mathrm{red}|s) \, \rangle = \int_{-\infty}^{\infty} \mathrm{d}s \, p(s) \, p(\mathrm{red}|s) = p(\mathrm{red}), \qquad (4)$$

which, using equation (3), implies

$$p(\mathrm{red}) = p(s > s_{\mathrm{red}}) = \frac{\mathrm{erfc}(s_{\mathrm{red}}/\sqrt{2})}{2}. \qquad (5)$$

Equation (3) gives a step-like dependence of the red fraction on concentration; in principle one could also imagine schemes where the red fraction increases with concentration in a continuous manner, but in this case it becomes more complicated to simultaneously ensure $\langle p(\mathrm{red}|s) \rangle = p(\mathrm{red})$ and $0 < p(\mathrm{red}|s) < 1$, due to the Gaussian integral in equation (4).

The parameter ρ lies between zero and unity and controls the strength of the correlation between the red fraction and concentration; we discuss its physical meaning below. Setting $\rho = 0$ gives us the uncorrelated case when the red fraction does not depend on parent halo concentration. Setting $\rho = 1$ on the other hand corresponds to 'complete correlation' where *all* galaxies in high(low)-concentration halos are labelled red (blue). The intermediate case $0 < \rho < 1$ clearly interpolates between these two extremes.

Having set up our model, we proceed by assigning colours to the galaxies. The red flag of the galaxy is chosen by drawing a uniform random number $u \in [0, 1)$ and setting the red flag to unity if $u < p(\mathrm{red}|s)$ and zero otherwise. Next, we draw a Gaussian random number $g - r$ from the appropriate red or blue distribution. In the basic S09 algorithm, the latter step also does not depend on parent halo concentration. In principle, we could once again use the values of s to introduce a further correlation between the actual $g - r$ values and halo concentration, but in practice it turns out to be difficult to do this while preserving the global colour distributions at fixed luminosity (which we must do since these are constrained by data). We therefore stick to the S09 procedure at this stage and draw from the appropriate 'red'/'blue' Gaussian without further correlation with concentration.

Ideally, we would correlate galaxy colours with the concentrations actually measured in the simulation. However, these concentrations are only approximately Lognormal, and deviations from the Lognormal shape render the second equality in equation (5) above invalid. Continuing to use $s_{\mathrm{red}} = \sqrt{2}\mathrm{erfc}^{-1}(2p(\mathrm{red}))$ then leads to the overall central and satellite red fractions not being preserved, with $\langle p(\mathrm{red}|s) \rangle \neq p(\mathrm{red})$. We could correct for this by calibrating the exact shape of $p(s)$ and numerically inverting the relation $p(s > s_{\mathrm{red}}) = p(\mathrm{red})$ to obtain s_{red}. Note, however, that what we are really interested in is not the actual shape of the distribution of concentrations, but only their *ranking* in halos of fixed mass. It is therefore easier to simply "Gaussianize" the measured log-concentrations, proceeding as follows.

(i) We first randomly draw a Gaussian variate s for each halo in the catalog and derive a Lognormal concentration c using equations (1) and (2).

---

[2] See Skibba (2009) for a comparison of central and satellite colours using mocks based on the S09 algorithm and in an earlier version of the Y07 catalog.
[3] $\delta_c(z)$ and $\sigma(m)$ are, respectively, the critical density for spherical collapse at redshift z and the r.m.s. of initial fluctuations smoothed on mass scale m, each extrapolated to $z = 0$ using linear theory.

(ii) Next, we bin the halos in 16 equi-log-spaced mass bins[4] and consider the lists of measured and Lognormal concentrations of halos in each bin. We rank order and reassign the Lognormal concentrations in a given bin according to the measured concentrations in that bin. In detail, if there are N halos in a bin, then the halo with the jth largest measured concentration is assigned the jth largest Lognormal concentration in this bin, with $j = 1, 2, \ldots, N$.

(iii) These reassigned Lognormal values of c are then used to distribute satellites in their respective parent halos, and the corresponding Gaussian values of s are used to induce conformity in the colours as described above, with s_{red} given by equation (5).

This ensures that galaxy colours in this model are assigned consistently and inherit the large scale environment dependence of assembly bias.

We will show that this procedure, which defines our default model, leads to differences in the satellite red fraction in groups with blue and red centrals (1-halo conformity) as well as specific spatial trends of galaxy red fractions around blue and red isolated objects well outside R_{200b} (2-halo conformity). As mentioned in the Introduction, it is also useful to ask how these trends would change if conformity arises not because of assembly bias, but due to some other halo property that *does not* show environmental trends. To this end, we will also consider a model in which galaxy colours are chosen and satellites are distributed exactly as in the default procedure above, except that we skip the rank ordering step (ii). This is equivalent to randomizing the halo concentrations at fixed halo mass before correlating them with the galaxy colours. In this model – which we will denote "*no-2h*" – we expect our mocks to exhibit 1-halo conformity without a corresponding 2-halo signal.

The parameter ρ has an interesting interpretation. It is easy to show that ρ satisfies the relations

$$\begin{aligned} \rho &= \frac{p(\mathrm{red}|s > s_{\mathrm{red}}) - p(\mathrm{red})}{1 - p(\mathrm{red})} \\ &\sim \frac{p(\mathrm{red}|\mathrm{old}) - p(\mathrm{red})}{1 - p(\mathrm{red})} \,. \end{aligned} \qquad (6)$$

where the second approximation holds if we assume that high concentration halos are old. Although simply a restatement of the definition of ρ in equation (3), equation (6) allows us to interpret ρ as a "quenching efficiency" (van den Bosch et al. 2008; Peng et al. 2010, 2012; Kovač et al. 2014; Phillips et al. 2014; Knobel et al. 2014). Written like this, in our default model ρ is the fraction of blue (or star forming) galaxies that became red (or quenched) because their respective parent halos grew old[5]. In the *no-2h* model, however, the connection between halo ages and galaxy colours is lost (since the former exhibit halo assembly bias at large scales while the latter will not), and the second relation in equation (6) will not hold. In each model of conformity, however, ρ can be thought of as a "group quenching efficiency", driven by the age of the parent halo of the group in the default model and by some local

but otherwise unspecified property of the group in the *no-2h* model.

Our scheme of generating concentration-dependent red flags smoothly interpolates between the uncorrelated case ($\rho = 0$) and the nearly 'completely correlated' case ($\rho = 1$). In practice, we perform this operation separately for satellites and centrals, which ensures that the overall central and satellite red fractions are left unaltered by construction. The model is flexible enough that, if needed, the group quenching efficiency ρ can be set separately for centrals and satellites, with the interpretation that different quenching mechanisms might play a role for centrals and satellites in the same halo. E.g., this might be the case if *sub*halo age is more relevant for satellite colour than the age of the parent halo (Hearin & Watson 2013). In this work, however, we do not explore this possibility and only use a one-parameter setup with ρ taken to be the same for centrals and satellites, independent of galaxy luminosity and halo mass. Galactic conformity arises from the fact that the colours of centrals and satellites in a group are affected by their common group concentration. The fact that the concentrations have a scatter at fixed halo mass means that the conformity will persist even when binning objects by the parent halo mass.

2.3 Calculating stellar masses

As a separate step, having assigned galaxy colours, we compute stellar masses using a colour dependent mass-to-light ratio that we have also fit to SDSS galaxies. In particular, we use

$$(M/L)_r = 4.66(g - r) - 1.36(g - r)^2 - 1.108 \,, \qquad (7)$$

to compute the $^{0.1}r$-band Petrosian mass-to-light ratio $(M/L)_r$ in units of $M_\odot/L_\odot$, and add a Gaussian 1-sigma scatter of 0.2 (we describe the procedure and data set used to obtain this fit in section 4). Taking the base-10 logarithm and adding $(M_r - 4.76)/(-2.5)$ gives us the log stellar mass in units of $h^{-2}M_\odot$. This does not guarantee that the central of a group, which is the brightest by construction, is also the most massive. In practice this affects about 8-10% of the groups in the total sample, with the actual number depending on the the value of ρ. This may be related to the findings of Skibba et al. (2011) regarding a non-zero fraction of groups in which the central is not the brightest; we will explore this further in future work.

3 SIMULATIONS

Our mocks are built on a suite of N-body simulations of cold dark matter (CDM), each of which resolves a periodic cubic box of comoving volume $(200h^{-1}\mathrm{Mpc})^3$ with 512^3 particles using our fiducial cosmology. This gives us a particle mass of $m_{\mathrm{part}} = 4.1 \times 10^9 h^{-1}M_\odot$. The simulations were run using the tree-PM code[6] GADGET-2 (Springel 2005) with a force resolution $\epsilon = 12.5h^{-1}\mathrm{kpc}$ comoving ($\sim 1/30$ of the mean particle separation) and a 1024^3 PM grid. Initial conditions were generated at $z = 99$ employing 2$^{\mathrm{nd}}$-order Lagrangian Perturbation Theory (Scoccimarro 1998), using the code[7] MUSIC (Hahn &

---

[4] The number of bins was chosen after testing for convergence.

[5] This can only be approximately correct, since, e.g., the present day population of blue satellites is not in general representative of the progenitors of all present day satellites. Our results do not depend on this interpretation, however, and one could simply treat ρ as a free parameter in the model.

[6] http://www.mpa-garching.mpg.de/gadget/

[7] http://www.phys.ethz.ch/~hahn/MUSIC/

Abel 2011) with a transfer function calculated using the prescription of Eisenstein & Hu (1998). We have run 10 realisations of this simulation by changing the random number seed used for generating the initial conditions and have used the resulting $z = 0$ snapshots for our mocks. The simulations were run on the Brutus cluster[8] at ETH Zürich.

To identify halos, we have used the code[9] ROCKSTAR (Behroozi et al. 2013b), which assigns particles to halos based on an adaptive hierarchical Friends-of-Friends algorithm in 6-dimensional phase space. ROCKSTAR has been shown to be robust for a variety of diagnostics such as density profiles, velocity dispersions, merger histories and the halo mass function. As mentioned earlier, we use the m_{200b} value reported by ROCKSTAR as the mass of the parent halo, and R_{200b} as its radius. We use the value of the halo scale radius r_s reported by ROCKSTAR to compute halo concentration $c_{200b} = R_{200b}/r_s$. The smallest halo mass we resolve sets the faintest luminosity we can reliably sample. We discard objects having $m_{200b} < 20\,m_{part}$, which allows us to set the luminosity threshold to $M_{r,max} = -19.0$. Having 10 independent simulations means that we can reliably characterise the sample variance on our observables for each mock configuration.

4   DATA

In this section we describe the data sets we use for comparison with the mocks, and give details of various fits used in defining the mocks.

4.1   The Y07 catalog

We base some of the fits required for generating our mocks (the colour distribution and satellite red fraction at fixed luminosity, and the mass-to-light ratio at fixed colour) on the galaxies contained in the Y07 group catalog[10]. These fits do not depend on the level of conformity, and we therefore additionally use the Y07 catalog as a baseline for galactic conformity as well. The Y07 catalog is built using the halo-based group finder described in Yang et al. (2005) to identify groups in the New York University Value Added Galaxy Catalog (NYU-VAGC; Blanton et al. 2005), based on the SDSS[11] (York et al. 2000) data release 7 (DR7; Abazajian et al. 2009). Throughout, we will only consider galaxies with spectroscopic redshifts ('sample II' of Y07) restricted to the range $0.01 < z < 0.07$, and also restrict the Petrosian absolute magnitudes to the range $-23.7 < M_r < -16$.

In part of the analysis below, we will use a luminosity-complete subsample – denoted "Y07-Lum" – containing galaxies with Petrosian absolute magnitudes $M_r < M_{r,max} = -19.0$ and Model $g - r$ colours from the NYU-VAGC as provided by Y07. Additionally, when comparing properties as a function of stellar mass, we will use another subsample – denoted "Y07-Mass" – containing values of Petrosian stellar mass $m_\star$ and Model $g - r$ colours obtained by running the KCORRECT_V4.2 code[12] of Blanton & Roweis (2007) on the corresponding Petrosian and Model properties, respectively, of the Y07 galax-
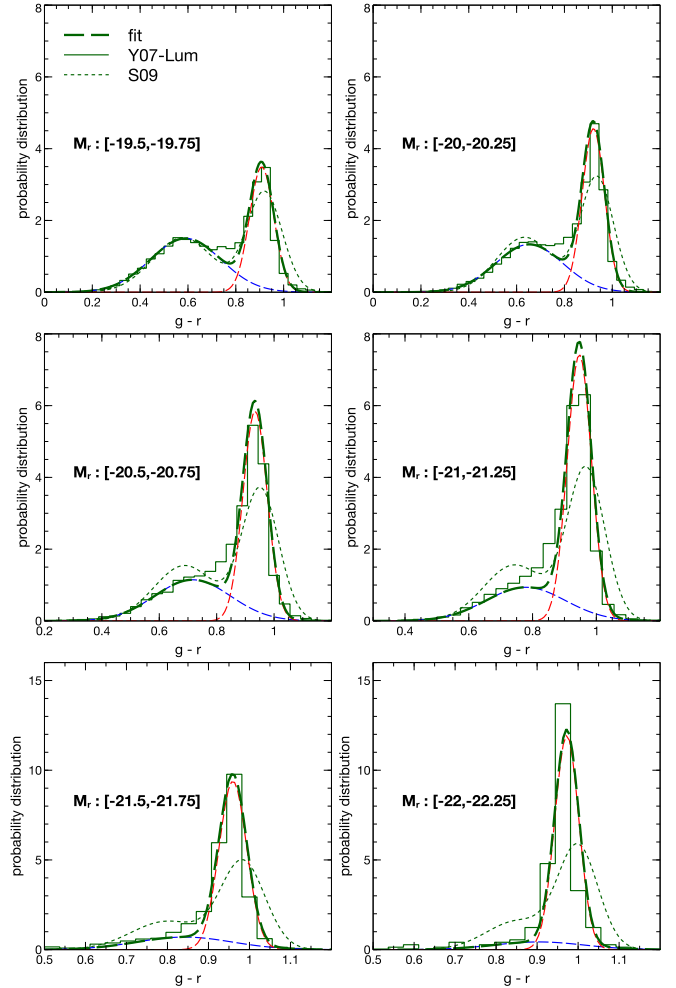
Figure 1. Comparison of observed Model $g - r$ distributions in bins of Petrosian M_r in the Y07-Lum catalog (solid green histograms) with the corresponding double-Gaussian fits reported in equations (9). We show the 'red' and 'blue' components in the fits as the respectively red and blue dashed lines, and the total of these as the dashed green lines. For comparison we show the S09 fits as dotted lines; the discrepancy between S09 and the Y07 catalog is most likely due to differences between DR7 and DR4 (which was used by S09) and our choice of using Model colours.

ies obtained from the MPA-JHU catalog[13] (Kauffmann et al. 2003) by matching galaxy IDs across the MPA-JHU and NYU catalogs. We use magnitudes that are K-corrected to their values at $z = 0.1$. We have checked that there is reasonable agreement between comparable galaxy properties in the NYU-VAGC and the MPA-JHU catalog. When showing mass functions and fractions, we apply inverse V_{max}-weighting to the galaxies in the Y07-Mass catalog.

Our choice of Petrosian quantities for defining both the stellar masses as well as the mass-to-light fit (see below) in the Y07-Mass catalog is motivated by the fact that the HOD we use has been calibrated on Petrosian absolute magnitudes by Zehavi et al. (2011). We have checked that there is reasonable agreement between Model and Petrosian stellar masses in the Y07-Mass catalog and, moreover, that the trends in the red fractions and associated observables which we discuss below
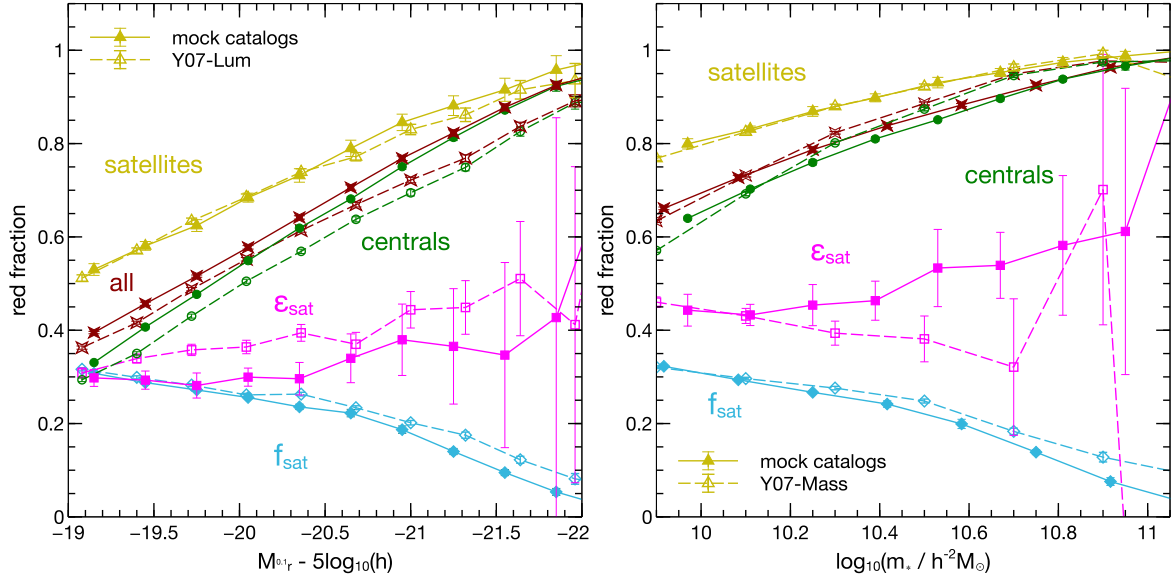
Figure 2. Conformity-independent variables as a function of luminosity *(left panel)* and stellar mass *(right panel)*. Filled symbols joined by solid lines show the results of averaging over 10 realisations of our mocks, while open symbols joined by dashed lines show measurements in the Y07 catalog. The error bars on the mock results show the r.m.s. fluctuations (standard deviation) around the mean value, while the errors on the Y07 data are estimated from 150 bootstrap resamplings. The cyan diamonds show the satellite fraction $f_{\rm sat}$. The dark red crosses, green circles and yellow triangles respectively show the red fractions for all galaxies ($f_{\rm red}$), only centrals ($f_{\rm red|cen}$) and only satellites ($f_{\rm red|sat}$). The magenta squares show the satellite quenching efficiency $\varepsilon_{\rm sat} = (f_{\rm red|sat} - f_{\rm red|cen})/(1 - f_{\rm red|cen})$. The 'red'/'blue' classification for both data and mocks uses equation (10) for the left panel and equation (11) for the right panel.

differ by only $\sim 10\%$ when using Model or Petrosian quantities. Consequently, we do not expect any of our qualitative conclusions to be affected by our choice.

4.2 Mass-to-light ratio fit

We fit a quadratic relation to the $^{0.1}r$-band Petrosian mass-to-light ratio $(M/L)_r$ at fixed value of Model $g - r$ colour in the Y07-Mass catalog. In particular, we compute the median value of $(M/L)_r$ in bins of $g - r$, using the median $g - r$ as the bin center. The resulting least-squares best fit is given in equation (7) and is close to but slightly lower than the one in equation (1) from Wang & White (2012). The measured r.m.s. scatter of $(M/L)_r$ in the bins of $g - r$ has an average value of 0.2 which we also use as described below equation (7).

4.3 Color-luminosity fits

We fit double-Gaussian shapes to the distributions of Model $g - r$ colours in bins of Petrosian absolute magnitude M_r in the Y07-Lum catalog. The resulting fits can be summarised using 5 quantities: the means and variances of the 'red' and 'blue' distributions and the probability $p(\mathrm{red}|M_r)$ that the colour is drawn from the 'red' distribution. The full $g - r$ distribution can then be written as

$$p(g - r|M_r) = p(\mathrm{red}|M_r)\, p_{\rm red}(g - r|M_r)$$
$$+ (1 - p(\mathrm{red}|M_r))\, p_{\rm blue}(g - r|M_r), \quad (8)$$

where, e.g., $p_{\rm red}(g - r|M_r)$ is Gaussian with mean $\langle g - r|M_r \rangle_{\rm red}$ and standard deviation $\sigma_{\rm red}(M_r)$, and similarly

for the blue distribution. We find the following best fit values:

$$p(\mathrm{red}|M_r) = 0.423 - 0.175\,(M_r + 19.5)$$
$$\langle g - r|M_r \rangle_{\rm red} = 0.9050 - 0.0257\,(M_r + 19.5)$$
$$\langle g - r|M_r \rangle_{\rm blue} = 0.575 - 0.126\,(M_r + 19.5)$$
$$\sigma_{\rm red}(M_r) = 0.0519 + 0.0085\,(M_r + 19.5)$$
$$\sigma_{\rm blue}(M_r) = 0.150 + 0.015\,(M_r + 19.5) \quad (9)$$

Figure 1 compares these analytic functions (dashed lines) with the measured $g - r$ distribution in the Y07-Lum catalog (solid histograms). For comparison, the dotted lines show the fits reported by S09 which were based on a similar catalog using DR4 of SDSS; these are rather different from the Y07-Lum data, which could be due to differences between the DR7 colours and those in DR4. (The discrepancy reduces but does not disappear if we use Petrosian colours.) Overall, we see a good agreement between the data and the fits, except for a "green valley" which is not captured by the sum of two Gaussians. In principle, one can obtain a better fit by introducing a third 'green' component (Krause et al. 2013; Carretero et al. 2015), but we choose not to do this here.

Although the algorithm classifies objects as red or blue depending on which Gaussian distribution their colours are drawn from, for ease of comparison with observational results, we will use sharp thresholds in $g - r$. When showing results as a function of luminosity we classify objects as red when their $g - r$ colour exceeds
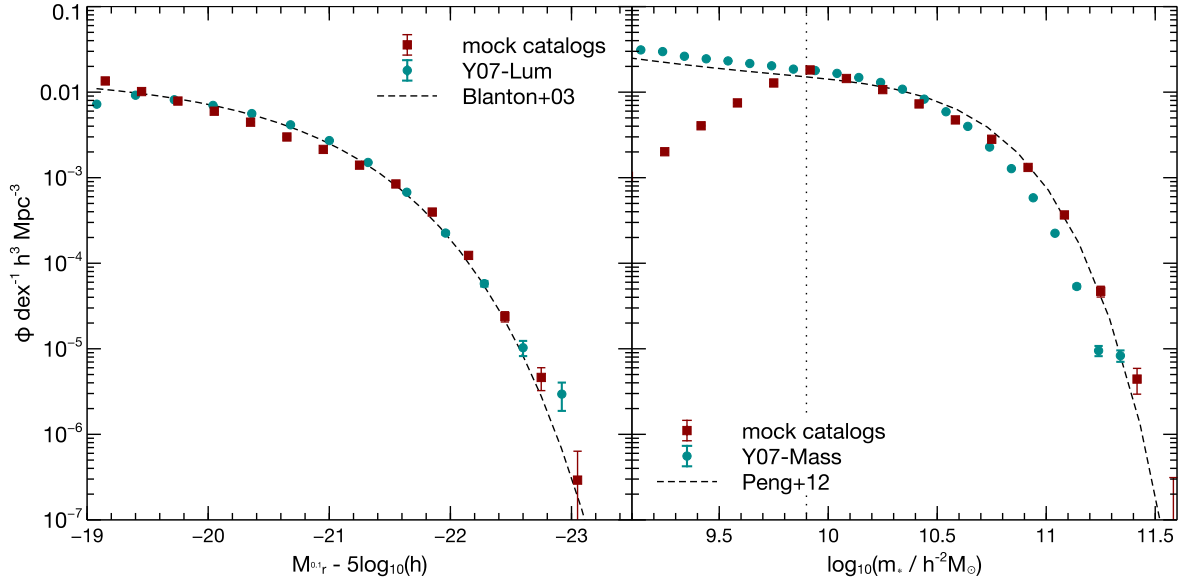
$$(g - r)_{\rm cut} = 0.8 - 0.03\,(M_r + 20), \quad (10)$$

and as blue otherwise (Zehavi et al. 2005). When showing results as a function of stellar mass we instead use the threshold

$$(g - r)_{\rm cut} = 0.76 + 0.10\,[\log_{10}(m_\star) - 10], \quad (11)$$

which is somewhat shallower than the threshold quoted by

Figure 3. All-galaxy luminosity *(left panel)* and stellar mass functions *(right panel)*. Red squares show the average over 10 independent mock catalogs, with error bars showing the r.m.s. scatter. Cyan circles show measurements in the Y07-Lum (left) and Y07-Mass catalogs (right), with errors estimated from 150 bootstrap resamplings. For comparison, the short-dashed black curve in the left panel shows the Schechter fit to the $^{0.1}r$-band luminosity function in SDSS data reported by Blanton et al. (2003), while the corresponding curve in the right panel shows the stellar mass function fit for the Y07 catalog as reported by Peng et al. (2012). The vertical dotted line in the right panel shows the approximate mass-completeness limit of our mocks at $\log_{10}(m_\star) = 9.9$.

van den Bosch et al. (2008) who use a slope of 0.15 instead of 0.1. We have found that equation (11) gives a slightly better separation of the bi-modal colour-mass distribution in the Y07-Mass catalog than the van den Bosch et al. (2008) relation does, although our qualitative conclusions do not depend on the choice of threshold. We apply the same threshold to colours in our mocks as well as in the Y07 data. Using sharp thresholds means that the measured red fractions $f_{\rm red}$ will, in general, differ from the probabilities $p({\rm red})$ discussed earlier.

5 RESULTS

We now present the results of our mock algorithm and compare them with corresponding measurements in the Y07 catalog. We start by discussing observables that *do not* depend on the presence or absence of conformity.

5.1 Conformity-independent observables

The following observables are independent of the level of conformity (i.e., the value of ρ) because their definition does not involve a simultaneous determination of central and satellite colour: the fraction of galaxies that are satellites ($f_{\rm sat}$), the average red fractions of all galaxies, centrals and satellites (respectively, $f_{\rm red}$, $f_{\rm red|cen}$ and $f_{\rm red|sat}$), and the satellite quenching efficiency $\varepsilon_{\rm sat} = (f_{\rm red|sat} - f_{\rm red|cen})/(1 - f_{\rm red|cen})$. Among these functions, the luminosity dependence of $f_{\rm sat}$ is determined solely by the HOD (which itself is fit using the luminosity dependence of clustering), that of $f_{\rm red}$ is fixed by the double-Gaussian fits[14], and the remaining quantities addition-

---

[14] Note that $f_{\rm red}$ depends on the actual shape of the double-Gaussian, not only on $p({\rm red}|M_r)$.

ally depend on the choice of satellite red fraction which we discuss next.

As mentioned previously, we restrict ourselves to a simple prescription in which $p({\rm red}|{\rm sat}, M_r)$ (the probability that $g-r$ for a satellite of luminosity M_r is drawn from the 'red' Gaussian) *as well as* the corresponding quantity $p({\rm red}|{\rm cen}, M_r)$ for centrals are independent of halo mass, in which case only one of these can be chosen independently. By comparing to the measured luminosity dependence of $f_{\rm red|sat}$, we find reasonable agreement using

$$p({\rm red}|{\rm sat}, M_r) = 1.0 - 0.33\left[1 + \tanh\left(\frac{M_r + 20.25}{2.1}\right)\right], \quad (12)$$

although this is by no means the only function that can do the job. This in turn fixes the luminosity dependece of $f_{\rm red|cen}$ and $\varepsilon_{\rm sat}$. The stellar mass dependence of all the quantities mentioned above is then also completely fixed.

The results of the comparison are shown in Figure 2, as a function of luminosity in the left panel and stellar mass in the right panel. The open symbols joined by dashed lines show the measurements in the Y07-Lum (left panel) and Y07-Mass catalogs (right panel), while the filled symbols joined by solid lines show the mean over 10 realisations of our mocks. The error bars on the mock data show the r.m.s. scatter (sample variance) of the respective quantities over all realisations, while the error bars on the Y07 data are estimated from 150 bootstrap resamplings. We see that, apart from systematic differences of $\lesssim 10\%$, there is good agreement between the mocks and the data. In particular, the mocks correctly reproduce the observed near-independence of $\varepsilon_{\rm sat}$ on stellar mass and luminosity, as well as matching its amplitude. The systematic differences could be due to one or more of the following: residual systematics in the HOD parameters and the mass-to-light fit, the fact that we do not exactly reproduce the observed colour distribution, and our choice of halo mass-independent central and satellite red fractions. In particular, the difference in $f_{\rm red}$
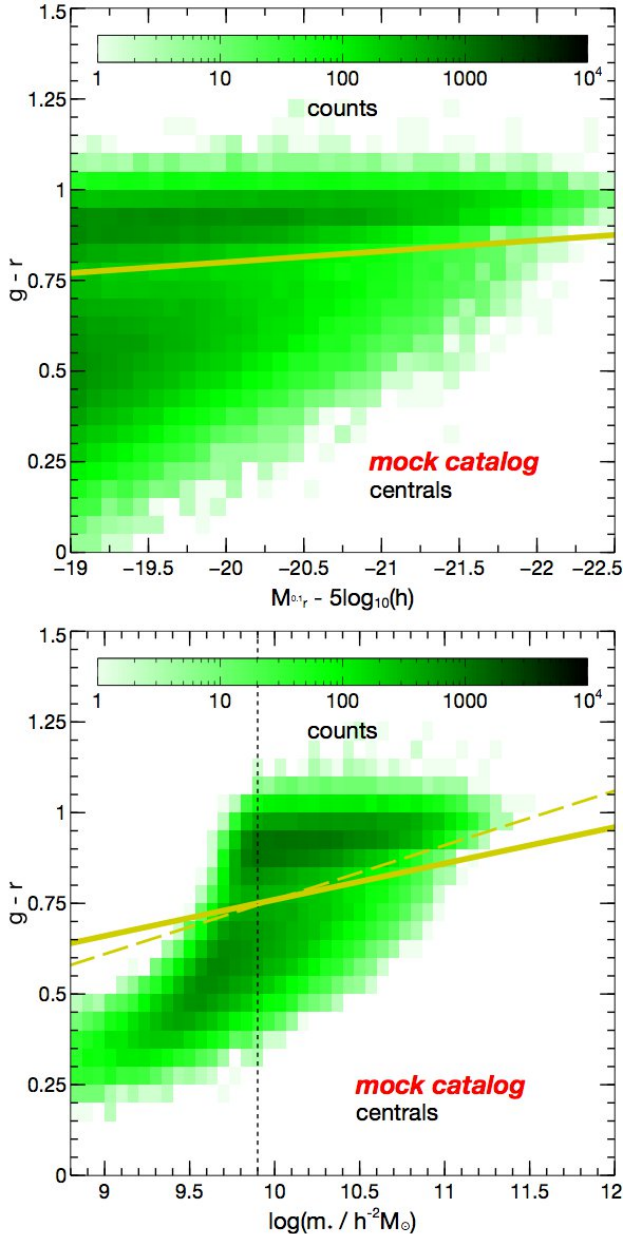
Figure 4. Number counts of centrals as a function of $g - r$ and luminosity *(top panel)* or stellar mass *(bottom panel)* in one of our mocks. We clearly see how a luminosity threshold propagates into a mass incompleteness for red objects. A visual inspection indicates that our mocks should be mass complete for $\log_{10}(m_\star) \gtrsim 9.9$ (vertical dotted line in the bottom panel). The thick yellow lines show equation (10) in the top panel and equation (11) in the bottom panel. For comparison, the dashed yellow line in the bottom panel shows the threshold used by van den Bosch et al. (2008).

is very likely due to the mismatch in the colour distributions around the "green valley" (see Section 4.3 and Figure 1). Since we match the satellite red fraction $f_{\rm red|sat}$ quite well by construction, the difference in $f_{\rm red}$ then also causes a difference in $f_{\rm red|cen}$.

Finally, an important set of observables that are independent of conformity are the luminosity and stellar mass functions of the mocks. Figure 3 compares these with corresponding measurements in, respectively, the Y07-Lum and Y07-Mass catalogs. We also show the fits to SDSS data re-

ported by Blanton et al. (2003) for the luminosity function and Peng et al. (2012) for the mass function. Overall there is good agreement between the measurements in our mocks, in the data and the corresponding fits from previous work; this serves as a sanity check on our algoritm. The fact that our measurements in the Y07-Mass catalog do not quite agree with the fits reported by Peng et al. (2012) highlights the fact that the shape and amplitude of the mass function is quite sensitive to the exact definition of stellar mass.

From a visual inspection, the mocks appear to be mass complete for $\log_{10}(m_\star) \gtrsim 9.9$, which is the threshold we will use below. For our choice of $h = 0.7$ in the N-body simulations, this corresponds to $\log_{10}(m_\star/M_\odot) > 10.2$. The incompleteness at lower masses is because our mock is luminosity complete with $M_r < -19.0$; the colour-dependence of the mass-to-light ratio (7) then means that we are missing most of the faint red galaxies (and many of the faint blue ones) that would populate the low mass end. This becomes clearer in Figure 4 which shows number counts of centrals as a function of $g - r$ and luminosity (top panel) or stellar mass (bottom panel) in one of our mocks. The deficit of low-mass red objects is clear in the bottom panel. Similar results hold for the satellites as well. Our choice of mass-completeness threshold is further justified by the fact that only $\sim 1\%$ of the galaxies with $\log_{10}(m_\star) > 9.9$ belong to the faintest bin $-19.2 < M_r < -19.0$, implying that fainter galaxies would contribute negligibly above this mass threshold.

5.2 Effects of correlating galaxy colour and halo concentration

We now investigate the effects of a non-zero value of ρ in observables that *do* respond to a correlation between central and satellite colours. To start with we simply explore the effects of changing the value of ρ, and later motivate a specific value by comparing to the Y07 catalog.

The left panel of Figure 5 shows $f_{\rm red|sat}$ as a function of satellite stellar mass, split by whether the corresponding central is red or blue, for two choices of $\rho = 0.01, 0.99$. For each of these choices, the points show the mean over 10 independent mocks. Since we are interested in understanding these mean trends in this plot, the error bars in both panels show the standard error on the mean (rather than the r.m.s. scatter). The plot clearly shows that a positive correlation goes in the direction of explaining conformity, which has been noted earlier by others as well. The open symbols (red triangles and blue inverted triangles) joined by dotted lines show the result of the algorithm setting $\rho = 0.01$, i.e. essentially no correlation, in keeping with what is usually assumed by standard HOD based algorithms. In this case there is no distinction between the two red fractions at the bright end, but fainter satellites with blue centrals are preferentially slightly redder than those with red centrals (a weak 'negative conformity'). We have checked that the latter effect is due to averaging over luminosities and completely disappears if we plot results at fixed luminosity instead[15] (not shown).

The filled symbols with solid/dashed lines show the result

---

[15] This traces back to our choice of satellite red fraction which is independent of halo mass. Had this not been the case, we would have seen a similar effect in the luminosity-based plot as well, arising in this case from an averaging over halo mass. The effect in the stellar mass plot would now be even more pronounced.
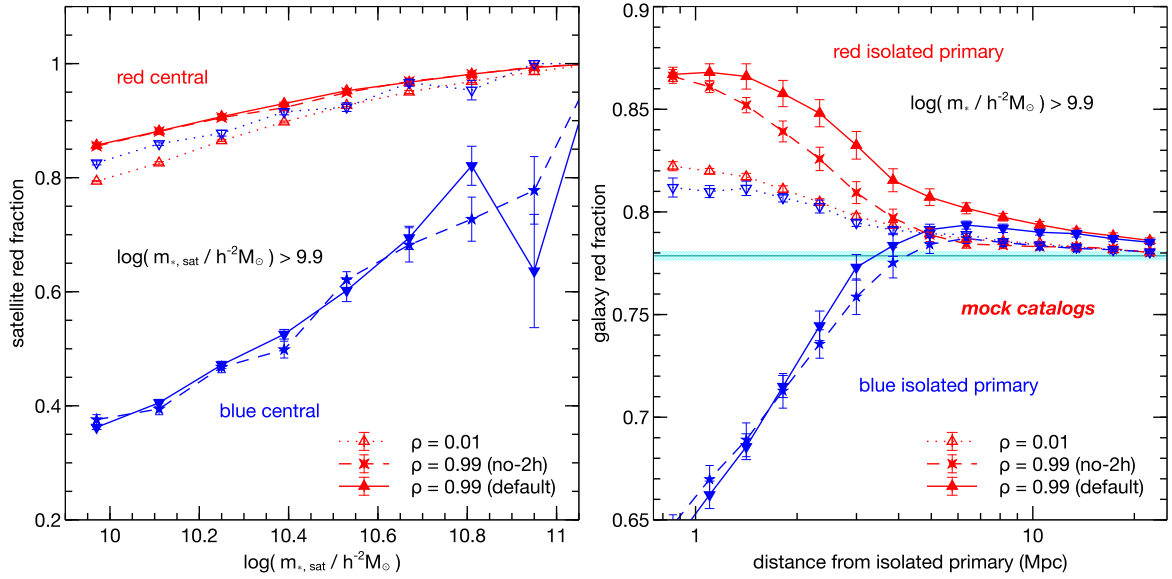
Figure 5. *(Left panel):* Satellite red fraction as a function of satellite stellar mass, split according to whether the associated centrals are red (red points and lines) or blue (blue points and lines). The open red triangles and blue inverted triangles with dotted lines show the result of the algorithm setting $\rho = 0.01$, i.e. essentially *no correlation* between galaxy colour and host halo concentration, as is routinely assumed by standard HOD based algorithms. The filled symbols with solid/dashed lines show the result when $\rho = 0.99$, i.e. *strong correlation*, in the presence (default model; red triangles and blue inverted triangles with solid lines) or absence (*no-2h* model; red crosses and blue stars with dashed lines) of 2-halo conformity as described in the text. The points show the mean over 10 independent mocks and the error bars the standard error on the mean. *(Right panel):* The red fraction of all galaxies surrounding red or blue "isolated primaries" as defined in the text, as a function of spherical distance, colour-coded and formatted as in the left panel, for the same set of 10 mocks used for the respective measurements in the left panel. All objects are required to have $\log_{10}(m_\star) > 9.9$ and we do not restrict the masses of their parent halos. The horizontal cyan line and band respectively show the average all-galaxy red fraction above this stellar mass threshold and its r.m.s. scatter over 10 independent mocks (these values are independent of ρ). Note that the scale on the vertical axis differs from that in the left panel. For both centrals and satellites, the distinction between red and blue was made using equation (11).
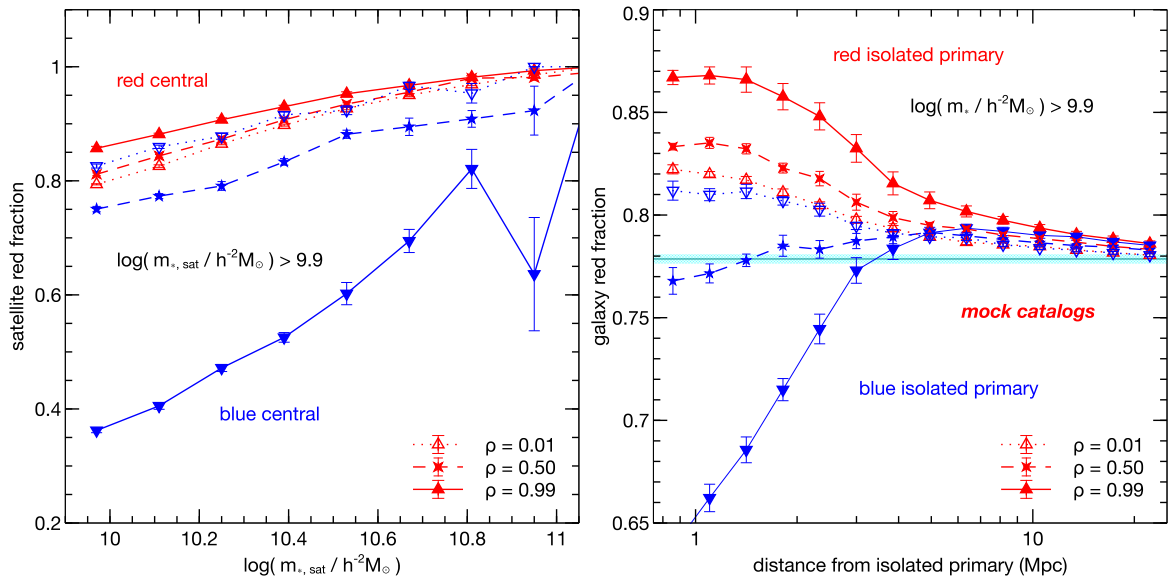
Figure 6. Same as Figure 5, except that the filled red crosses and blue stars joined by dashed lines now show the result for mocks with the default model, but where we set $\rho = 0.5$ ("medium" correlation between colour and concentration). The open triangles with dotted lines and filled triangles with solid lines are the same as in Figure 5. This plot demonstrates the tunability of our model, which is one of our key results.
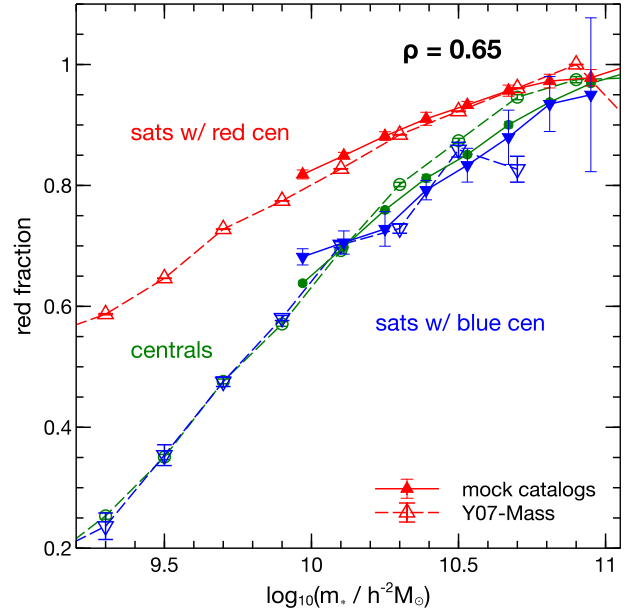
when $\rho = 0.99$, i.e. strong correlation. In this case satellites with red centrals are clearly significantly redder than satellites with blue centrals. The filled red triangles and blue inverted triangles joined by solid lines show the result for mocks that used our default model of conformity, rank ordering the Lognormal halo concentrations according to the measured concentrations from the simulation in 16 equi-log-spaced mass bins (see Section 2.2). The red crosses and blue stars with dashed lines show the result for mocks that used the *no-2h* model, with randomly assigned Lognormal concentrations. As expected, the red fractions for these two cases are nearly identical.

The right panel of the Figure is formatted identically to the left panel and uses the same set of mocks. In this case, we show the red fraction of all galaxies with $\log_{10}(m_\star) > 9.9$ as a function of their distance r from red or blue "isolated primaries"; we define the latter as galaxies of mass $m_\star$ that do not have any galaxy more massive than $m_\star/2$ within a spherical radius of 500kpc[16]. We find that the galaxies picked by this definition are predominantly centrals, with $\sim 10\%$ of isolated primaries being satellites (see also Hearin et al. 2015). We consider isolated primaries in order to be close to the selection criteria used in recent observational studies (see, e.g., Kauffmann et al. 2013). We investigate the impact of changing the selection criterion in Appendix A2.

The horizontal cyan line and associated band respectively show the mean and r.m.s. scatter over 10 realisations of the average all-galaxy red fraction which is independent of conformity strength. The mocks with $\rho = 0.01$ show nearly identical trends at $r \gtrsim 2$Mpc regardless of the colour of the isolated primary, although the red fractions remain above the global value even as far as 10Mpc from the center. There is a weak, conformity-like signal at small separations, which we have checked is entirely due to averaging over halo mass and disappears when using galaxies in fixed bins of halo mass. Together with the apparent 'negative conformity' seen for this set of mocks in the left panel, this reiterates the need to be cautious when interpreting trends in analyses that average over luminosity and halo mass.

Unlike the left panel, the two sets of mocks with $\rho = 0.99$ now show distinct trends. In the *no-2h* mocks, the red fractions around blue and red isolated primaries are different until a distance of ~ 4Mpc from the center (the one around red isolated primaries being higher), beyond which they are identical and also coincide with the "no conformity" red fractions associated with $\rho = 0.01$. The default mocks, on the other hand, show a similar but substantially larger difference between the red fractions out to ~ 6Mpc, beyond which they are also nearly identical but substantially larger than the red fractions in the other data sets (see section 6 and Appendix A2 for a discussion of these trends).

Figure 6 shows the same quantities as Figure 5, except that the filled red crosses and blue stars joined by dashed lines now show the results for default mocks where we set $\rho = 0.5$ (medium correlation). This plot shows how the difference between the red fractions around blue and red centrals/isolated primaries changes with group quenching efficiency ρ and demonstrates the tunability of our model, which is one of our key results.

5.3 Fixing the level of conformity

We notice in the left panel of Figure 6 that the red fraction $f_{\rm red|sat,bc}$ of satellites with blue centrals is particularly sensitive to the value of ρ. This happens, at least in part, due to the inherent asymmetry of satellite colours, most of which are red. Consequently, we can use measurements of 1-halo conformity in the Y07 catalog to fix the value of ρ, which can then be used to *predict* the 2-halo conformity signal.

By trial and error we have found that setting ρ within $\sim 10\%$ of $\rho = 0.65$ leads to a behaviour of $f_{\rm red|sat,bc}$ in the mocks that closely resembles the one in the data over the mass range allowed by the mocks. Figure 7 shows red fractions averaged over 10 mocks that used $\rho = 0.65$, and we see that both $f_{\rm red|sat,bc}$ and $f_{\rm red|sat,rc}$ agree very well with the Y07 measurements. The results of the previous section show that this agreement is independent of whether we use the default or the *no-2h* model. Notice that the red fraction of satellites with blue centrals $f_{\rm red|sat,bc}$ in both data and mocks is remarkably similar to the corresponding $f_{\rm red|cen}$. This is particularly true for the data at low masses where our current mocks do not reach.

Figure 8 shows the large scale conformity signal predicted in the mocks having $\rho = 0.65$, using both the default and the

Figure 7. Comparison of "conformity red fractions" $f_{\rm red|sat,rc}$ and $f_{\rm red|sat,bc}$ of satellites having red and blue centrals, respectively, with the red fraction of centrals $f_{\rm red|cen}$, for the Y07-Mass catalog (open symbols joined by dashed lines) and in mocks that used $\rho = 0.65$ (filled symbols with solid lines). The red triangles, blue inverted triangles and green circles respectively show $f_{\rm red|sat,rc}$, $f_{\rm red|sat,bc}$ and $f_{\rm red|cen}$ (the last are the same as in Figure 2). The error bars on the mock results show the r.m.s. fluctuations around the mean value over 10 realisations, while the error bars on the Y07 data are estimated from 150 bootstrap resamplings. Notice the remarkable similarity between $f_{\rm red|sat,bc}$ and $f_{\rm red|cen}$, especially at small masses in the Y07-Mass catalog.

---

[16] This definition is somewhat different from the observationally-motivated one employed by Kauffmann et al. (2013), who used a cylinder in redshift space and projected distance (see also Hearin et al. 2015). In this paper, however, we do not compare our 2-halo results with observations, and the simpler 3-dimensional definition above suffices to understand various trends in the signal. The signal itself is expected to diminish in strength due to projection effects.
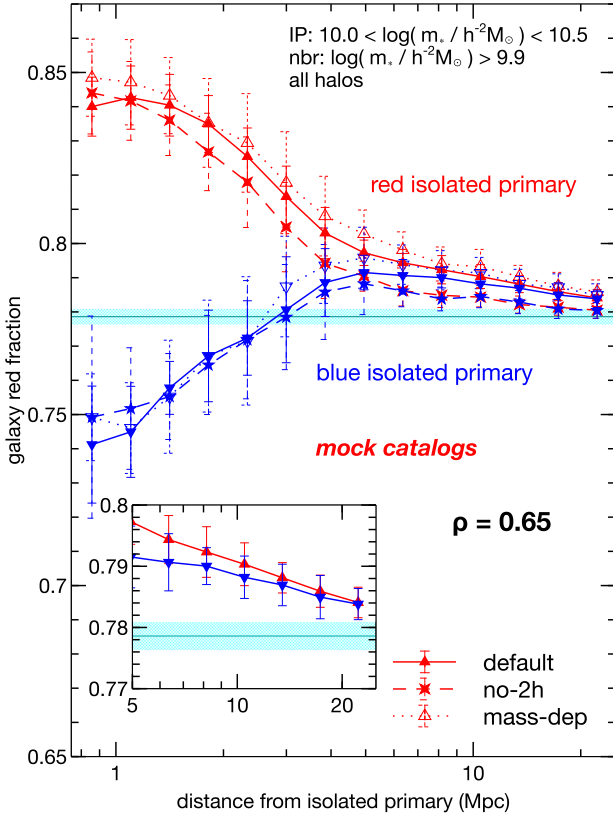
Figure 8. Large scale conformity predicted in three configurations of mocks that used $\rho = 0.65$ and whose respective 1-halo conformity signals are each consistent with measurements in the Y07 catalog. Filled symbols (red triangles and blue inverted triangles) with solid lines used our default mocks with halo mass-independent satellite and central red fractions at fixed luminosity, in which 2-halo conformity is switched on. Filled symbols (red crosses and blue stars) with dashed lines used the *no-2h* mocks in which 2-halo conformity is switched off. Finally, open symbols (red triangles and blue inverted triangles) with dotted lines used mocks in which 2-halo conformity was switched on and the red fraction of centrals at fixed luminosity had an additional dependence on halo mass as described in Appendix A1. The error bars on the mock results show the r.m.s. fluctuations around the mean value over 10 realisations for each configuration. The inset zooms in on the behaviour of the signal in the default mocks at very large separations. Unlike Figures 5 and 6, we restrict the isolated primaries to lie in the stellar mass range $10.0 < \log_{10}(m_\star) < 10.5$, while their neighbours are required to have $\log_{10}(m_\star) > 9.9$. The horizontal cyan line and band respectively show the average all-galaxy red fraction above the latter mass threshold and its r.m.s. scatter over 10 independent mocks (these values are independent of ρ).

no-2h models. To assess the effect of our assumption of mass-independent satellite and central red fractions, we also show the corresponding signal in mocks having 2-halo conformity, but in which the red fraction of centrals is mass-*dependent* as described in Appendix A1. These were constructed to match the conformity-independent observables discussed earlier, as well as the 1-halo conformity signal, for which it suffices to use $\rho = 0.65$ again (see Figure A1). In each case, we restrict the stellar mass of the isolated primaries to lie in the range $10.0 < \log_{10}(m_\star) < 10.5$. We see that the overall signal in all three mocks is very similar at scales $\lesssim 4$Mpc. At larger scales, the mocks with a halo mass dependent central red fraction show a slightly higher signal than in our default mocks. The

large scale signal in the *no-2h* mocks, on the other hand, is noticeably smaller than in the default. The inset zooms in on the behaviour of the signal in the default mocks at very large separations. The error bars depict the r.m.s. fluctuations around the mean over 10 realisations for each configuration.

Figure 9 shows a break-down of these large scale trends as a function of halo mass. Each panel shows the results for our default and *no-2h* mocks (formatted identically to Figure 8 and with the same restrictions on stellar masses of the isolated primaries and their neighbours), with the top left panel showing the same configuration as Figure 8 and the top right, bottom left and bottom right panels showing bins of increasingly larger halo mass. Each panel shows the average all-galaxy red fraction in the respective halo mass bin, and its r.m.s. scatter, as the horizontal cyan line and band, respectively. We clearly see that the large difference between red fractions at separations $\lesssim 4$Mpc arises primarily from large halo masses, while the distinction between the default and *no-2h* signal at $\gtrsim 8$Mpc only emerges at the smallest halo masses. We discuss these results in section 6 below.

6   DISCUSSION

The 1-halo conformity trends seen in the left panels of Figures 5 and 6, and in the mock results in Figure 7 are a straightforward consequence of our choice of implementation and the definition of the group quenching efficiency ρ as discussed in section 2.2. As ρ increases and approaches unity in our model, red (blue) satellites preferentially live in halos hosting red (blue) centrals. An interesting aspect of Figure 7 is the remarkable similarity of the red fraction of satellites with blue centrals and the red fraction of centrals at low stellar mass. A similar result was obtained by Phillips et al. (2014), who found that the SFRs of satellites with star forming centrals are essentially the same as those of isolated galaxies with similar stellar mass. This would imply that the quenching efficiencies $\varepsilon_{\mathrm{sat|SFc}}$ of the satellites with star forming centrals are consistent with being zero. On the other hand, Knobel et al. (2014) reported values of $\varepsilon_{\mathrm{sat|SFc}}$ different from zero. This apparent discrepancy is possibly due to differences in the sample definitions in these two studies; in particular, unlike Phillips et al. (2014), Knobel et al. (2014) limited their analysis to satellites residing in groups with at least 3 members with $m_\star > 10^{10} M_\odot$, thereby removing many low mass groups from the sample. As Knobel et al. (2014) also report a strong positive dependence of $\varepsilon_{\mathrm{sat}}$ on halo mass, it is natural to expect that the quenching efficiency in a sample biased toward more massive haloes would be nonzero. It will be very interesting to extend our mocks to lower stellar masses using a higher resolution simulation and compare the resulting 1-halo conformity trends – particularly those at fixed group richness and halo mass – with the data, but this is beyond the scope of the present work.

Turning to the large scale trends of red fractions surrounding isolated primaries, we encounter an even richer picture. It has been argued in the recent literature that large scale differences between red fractions or mean star formation rates surrounding blue and red isolated primaries must arise from environmental correlations across different halos (Kauffmann et al. 2013) and are therefore a signal of 2-halo conformity (Hearin et al. 2015). Our results in Figure 5 and especially Figure 8, however, show that an alternative explanation is also possible. Figure 8 used three different sets of mocks, *all* of which are constructed to give a 1-halo conformity signal consistent with
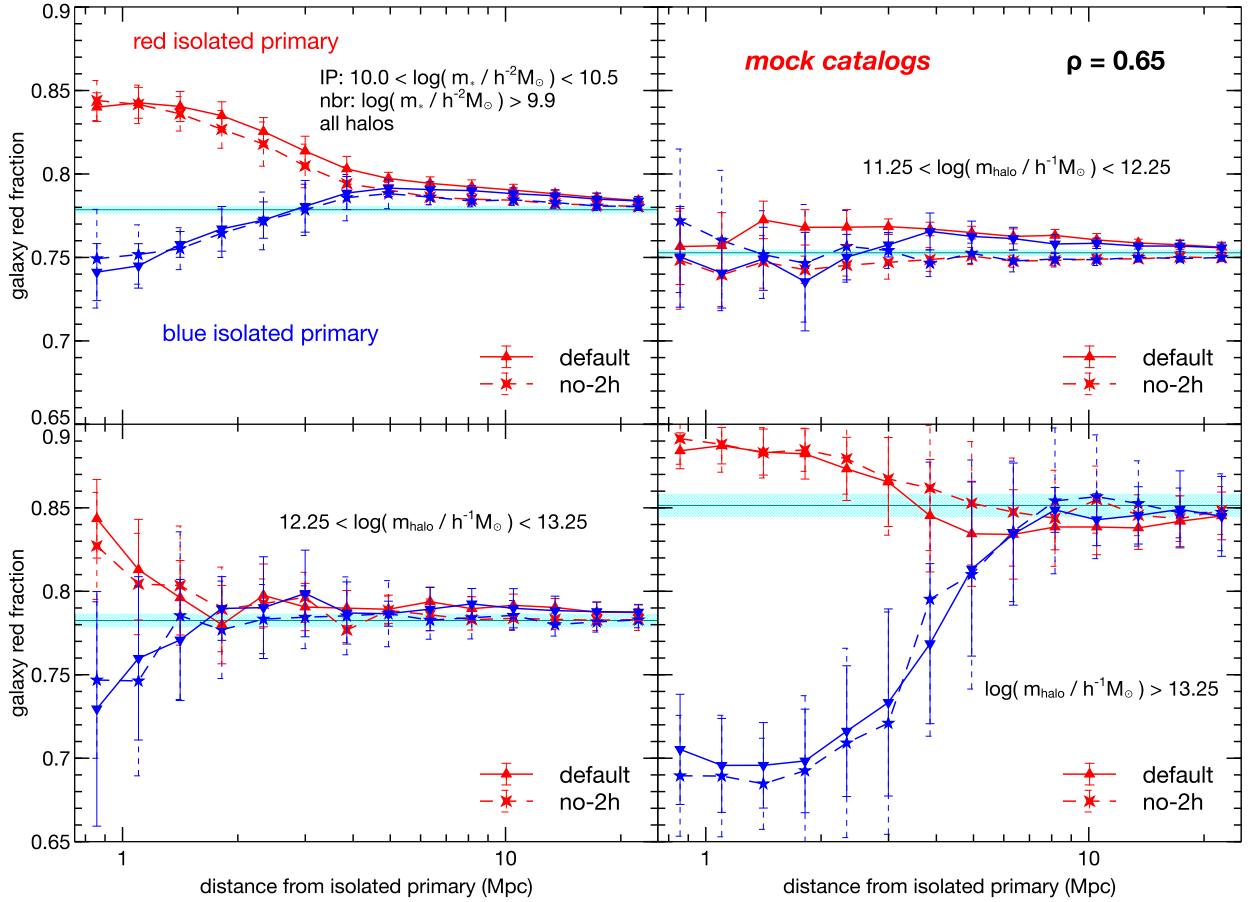
Figure 9. Large scale conformity signal for $\rho = 0.65$, broken down by halo mass as indicated. Note that the mass restrictions apply to the parent halos of both the isolated primary as well as its neighbours. Each panel is formatted identically to Figure 8 and shows the results for the default and *no-2h* mocks. See text for a discussion.

measurements in the Y07 catalog. Only two of these mocks have a genuine 2-halo conformity built in, however; the third contains randomly assigned halo concentrations which are not correlated with the halo environment. This third set of *no-2h* mocks serves as a useful toy example of the possibility that conformity might arise due to some property of halos that *does not* exhibit large scale environmental effects (see the discussion in the Introduction). The large scale conformity signal for all three mocks is *very similar at scales* $\lesssim$ 4Mpc. Figure 9 shows that the difference of red fractions at these scales is dominated by halo masses $\log_{10}(m) \gtrsim 13.25$ (bottom right panel) – for which it is consistent with being a 1-halo effect[17] – and has a smaller and noisier contribution from small halo masses (top right panel, see also Appendix A2). This means that, at these scales, we could easily mistake a purely 1-halo effect for genuine 2-halo conformity[18] Similar conclusions can be drawn by comparing the $\rho = 0.99$ measurements in the right panel of Figure 5 with those in the mocks with $\rho = 0.01$ or no conformity. The $\rho = 0.99$ *no-2h* measurements are identical to

the $\rho = 0.01$ measurements at large scales, which is expected since neither of these mocks has any 2-halo conformity. The measurements in the two $\rho = 0.99$ mocks on the other hand are very similar at scales $\lesssim$ 4Mpc. Taken together, this shows that that the conformity signal at $\lesssim$ 4Mpc in the $\rho = 0.99$ mocks is almost entirely a 1-halo effect (see Appendix A2 for further discussion).

From the observational point of view, halo mass-dependencies can in principle be controlled by performing tests at, e.g., fixed group richness (Koester et al. 2007; Skibba et al. 2007; Skibba 2009), stellar mass of the central (More et al. 2011) or any other observable property that correlates well with halo mass (Lu et al. 2015). Notice, however, that all the measurements in Figures 8 and 9 use isolated primaries with stellar masses $10.0 < \log_{10}(m_\star) < 10.5$ and still cannot distinguish between the default and *no-2h* models at scales $\lesssim$ 4Mpc, unless the halo mass is explicitly restricted to small values. We have also checked that the relative behaviour of our models at these scales remains unchanged when using primaries of different stellar mass[19]. This is unfortunate, since it very likely means that one cannot conclusively argue that the conformity measured by Kauffmann et al. (2013) at projected scales

---

[17] For comparison, a cluster-sized halo of mass $10^{14}h^{-1}M_\odot$ has a radius $R_{200b} \simeq 1.7$Mpc for our cosmology, and the largest halos in our simulations reach masses of $\sim 10^{14.8}$-$10^{15.2}h^{-1}M_\odot$.

[18] Figure 8 also shows that the large scale conformity signal appears to be robust against a mass dependence of the central red fraction, showing a slight increase on average as compared to the default mocks.

[19] Figure A3 in the Appendix shows that the signal, particularly at large scales, is essentially independent of the stellar mass of the primary; we attribute this to a large scatter in the distribution of halo masses at fixed stellar mass (Figure A4).

$\lesssim$ 4Mpc in similar mass bins is evidence of galaxy assembly bias. Projection effects are unlikely to alter this conclusion. It will be useful to repeat such tests at fixed group richness, which might be a better indicator of halo mass.

For now, it is very interesting to note that there *is*, in fact, a signal which diminishes in the absence of genuine 2-halo conformity and is also robust against the inclusion of halo mass dependence in the red fractions. This is the fact that, in the presence of 2-halo conformity, the red fractions at *even larger* scales ($\gtrsim$ 8Mpc) surrounding both red and blue isolated objects *remain above the global average value* by a small but statistically significant amount, showing nearly identical values and a trend that is relatively insensitive to the halo mass dependence of the central red fraction. When genuine 2-halo conformity is *absent*, the red fractions at these scales are discernably closer to the global average; as noted earlier, they are also identical to the "no conformity" red fractions at these scales. These trends can be seen in Figures 5, 8 and A2, with the elevation compared to the global value seen clearly in the zoom-in inset panel of Figure 8. Figure 9 shows that this signal is absent at large halo masses and only emerges in the range $11.25 < \log_{10}(m) < 12.25$.

This dependence on halo mass is exactly what one expects from a signal driven by halo assembly bias; in fact, one can also derive a more detailed understanding of the *nature* of the signal using the Halo Model. In Appendix A2, e.g., we argue that the red fractions at very large separations from central galaxies are determined by ratios of cross-correlation functions of red/blue galaxies with red/blue centrals, in which the concentration-dependence of halo assembly bias couples with that of galaxy colour introduced in our default model and leads to an elevation that is qualitatively similar to what we see in Figure 8. The fact that the signal is only of order a few percent is consistent with halo assembly bias being a weak effect.

Our model assumes that central galaxies are always the brightest members of their respective groups, and we have also imposed this condition when defining centrals in the Y07 catalog. A number of studies indicate that this is not a good assumption for a substantial fraction of groups (see, e.g., Skibba et al. 2011; Masaki et al. 2013a; Hikage et al. 2013). Since galactic conformity manifests as a *similarity* of galaxy colours in groups, any errors in classifying galaxies as centrals and satellites, provided they have a minimal impact on overall group membership, will tend to make these populations similar to each other and are therefore likely to *induce* conformity-like effects (Campbell et al. 2015). Consequently, it is possible that our analysis in Section 5.3 somewhat overestimates the strength of conformity (i.e., the value of ρ). However, the results of Section 5.2 suggest that our conclusions regarding the *relative* strengths of the conformity signal at various scales are qualitatively robust to such errors. It will nevertheless be interesting to revisit this issue in future work using more refined criteria for identifying centrals.

A proper comparison with data will require accounting for projection effects both in the red fraction measurements as well as the definition of isolated primaries themselves. Although these will dilute the signal, its strength should also increase upon including galaxies with smaller stellar masses (and stronger assembly bias) than we could access in our mocks, and overall we expect that the difference between large scale 1-halo and genuine 2-halo effects will remain measurable. Additionally, we expect that simultaneous measurements of 1-halo and

large scale conformity together with colour-dependent clustering will be required to break the weak degeneracy between halo mass dependence of the central red fraction and the level of conformity. Such a joint analysis will also be important from the point of view of obtaining unbiased HOD fits that account for galactic conformity (Zentner et al. 2014).

7 SUMMARY AND CONCLUSIONS

We have introduced a flexible model of galactic conformity within the Halo Occupation Distribution (HOD) framework by modifying and extending the algorithm described by Skibba & Sheth (2009). By construction, our mock galaxy catalogs show good agreement with measurements of conformity-*independent* variables in the Yang et al. (2007, Y07) group catalog based on DR7 of the SDSS. These variables include the satellite fraction, the red fractions of all galaxies, centrals and satellites, and the satellite quenching efficiency $\varepsilon_{\rm sat}$ (Figure 2), as well as the all-galaxy luminosity and stellar mass functions (Figure 3). Galaxy luminosities are assigned using the HOD (we use the calibration by Zehavi et al. 2011), colours are assigned using colour-luminosity fits to SDSS data (Figure 1 and equations 9) and stellar masses are assigned using a colour-dependent mass-to-light ratio (equation 7), also fit to SDSS data. Our mock catalogs are luminosity-complete for $M_r < -19.0$ and mass-complete for $\log_{10}(m_\star) \gtrsim 9.9$ (Figures 3 and 4).

Our algorithm introduces conformity between the colours of the central and satellites of a group (a 1-halo effect) by using a tunable group quenching efficiency ρ to correlate these colours with the concentration of the parent dark halo of the group. Halo concentration (which has a scatter at fixed halo mass) is therefore identified as the "hidden variable" in our model which causes galactic conformity even in halos of fixed mass. Halo assembly bias then leads to a 2-halo effect at very large scales (this is our default model), which we can also switch off by randomizing halo concentrations among halos of fixed mass (we call this the *no-2h* model). The latter is a useful toy example in which conformity arises due to some unspecified property of halos (e.g., this might be a coupling between star formation activity and the hot gas content in a halo) that *does not* exhibit large scale environmental effects. We have performed various tests to study the nature of the signal, including changing ρ (Figure 6) in the presence or absence of 2-halo conformity (Figure 5) for different choices of isolation criteria – we used isolated primaries (Figures 5 and 6) as well as group centrals (Figure A2). Our main results can be summarized as follows.

- We find that setting $\rho = 0.65$ gives a 1-halo conformity signal in the mocks which agrees well with the corresponding signal in the Y07 catalog (Figure 7). The signal manifests as a difference between the red fractions of satellites in groups with red and blue centrals. Additionally, in the Y07 catalog, the red fraction of satellites with blue centrals is remarkably similar to the red fraction of centrals at all masses; our mocks correctly reproduce this trend down to their completeness limit.
- The above value of ρ also leads to a signal at large scales in the mocks (Figure 8); specifically, we see a significant difference between the galaxy red fractions surrounding red and blue isolated primaries out to separations $\lesssim$ 4Mpc. Interestingly, we find that this signal is dominated by the 1-halo contribution of large halos with $\log_{10}(m) > 13.25$ (Figure 9),

and *persists even when we switch off 2-halo conformity* in our *no-2h* model. This implies that the observation of such a difference (e.g. Kauffmann et al. 2013) is not conclusive evidence that galactic conformity arises from halo assembly bias, since it could also arise from 1-halo effects "leaking" to large scales due to averaging over halo mass (section 6).

• At even larger scales ($\gtrsim$ 8Mpc in Figure 8), the signals with and without 2-halo conformity *do* become distinct, with the genuine 2-halo signal remaining *significantly elevated* compared to the global average red fraction out to separations in excess of 15Mpc (at least in the 3-d case that we consider). This 2-halo signal is absent at large halo masses and only emerges at smaller masses $11.25 < \log_{10}(m) < 12.25$ (Figure 9), being qualitatively consistent with expectations from halo assembly bias (section 6 and Appendix A2). We therefore suggest that this elevation compared to the global average could be a more robust indicator of large scale galaxy assembly bias than is the difference between red fractions at scales $\lesssim$ 4Mpc.

We end with a brief discussion of future extensions of our work. In a forthcoming paper (Kovač et al., in preparation), we will compare the large scale signal in our mocks, after accounting for projection effects, with a corresponding measurement in the Y07 catalog to determine whether or not the observed large scale conformity is due to galaxy assembly bias or a residual of some other 1-halo process. Tests at fixed group richness will also be useful in answering this question. It will also be interesting to explore the use of galaxy lensing and/or traditional correlation function analyses to validate the connection between galaxy colours and host halo concentrations assumed in this work, particularly to check for consistency with the value of ρ presented above. In another publication (Pahwa et al., in preparation), we will present the analytical formalism for including conformity in the HOD framework; we will show that this requires straightforward modifications in existing HOD pipelines.

Our algorithm can also be extended to include radial profiles for satellite velocity dispersions and colours (Prescott et al. 2011; Hartley et al. 2015), as well as concentration-dependent satellite abundances (Wechsler et al. 2006; Mao et al. 2015). The signal at high redshift is interesting too; this could be modelled using analytical prescriptions tuned to match high-redshift luminosity function and clustering data (Tacchella et al. 2013; Behroozi et al. 2013a; Jose et al. 2014). Finally, it will be extremely interesting to extend our algorithm to lower stellar masses using accurate faint-end ($M_{r,\max} \sim -16.0$) HOD fits and higher resolution N-body simulations. We estimate that a simulation with 1024^3 particles in a $(100h^{-1}\mathrm{Mpc})^3$ box will allow us to create catalogs that are mass-complete for $\log_{10}(m_\star) \gtrsim 8.7$; comparing these to data will provide us with stringent tests on the nature of the conformity signal.

REFERENCES

Abazajian K. N. et al., 2009, ApJS, 182, 543
Balogh M. L., Morris S. L., 2000, MNRAS, 318, 703
Baugh C. M., 2006, Reports on Progress in Physics, 69, 3101
Behroozi P. S., Wechsler R. H., Conroy C., 2013a, ApJ, 770, 57
Behroozi P. S., Wechsler R. H., Wu H.-Y., 2013b, ApJ, 762, 109
Berlind A. A. et al., 2006, ApJS, 167, 1
Berlind A. A., Weinberg D. H., 2002, ApJ, 575, 587
Birrer S., Lilly S., Amara A., Paranjape A., Refregier A., 2014, ApJ, 793, 12
Blanton M. R. et al., 2003, ApJ, 592, 819
Blanton M. R., Roweis S., 2007, AJ, 133, 734
Blanton M. R. et al., 2005, AJ, 129, 2562
Bullock J. S., Kolatt T. S., Sigad Y., Somerville R. S., Kravtsov A. V., Klypin A. A., Primack J. R., Dekel A., 2001, MNRAS, 321, 559
Campbell D., van den Bosch F. C., Hearin A., Padmanabhan N., Berlind A., Mo H. J., Tinker J., Yang X., 2015, MNRAS, 452, 444
Carollo C. M. et al., 2014, ArXiv e-prints: 1402.1172
Carretero J., Castander F. J., Gaztañaga E., Crocce M., Fosalba P., 2015, MNRAS, 447, 646
Cen R., 2014, ApJ, 781, 38
Cooray A., Sheth R., 2002, Phys. Rep., 372, 1
Coupon J. et al., 2015, MNRAS, 449, 1352
Croton D. J. et al., 2006, MNRAS, 365, 11
Dalal N., White M., Bond J. R., Shirokov A., 2008, ApJ, 687, 12
Deason A. J., Conroy C., Wetzel A. R., Tinker J. L., 2013, ApJ, 777, 154
Desjacques V., 2008, MNRAS, 388, 638
Eisenstein D. J., Hu W., 1998, ApJ, 496, 605
Fabian A. C., Sanders J. S., Allen S. W., Crawford C. S., Iwasawa K., Johnstone R. M., Schmidt R. W., Taylor G. B., 2003, MNRAS, 344, L43
Fakhouri O., Ma C.-P., 2010, MNRAS, 401, 2245
Gao L., Springel V., White S. D. M., 2005, MNRAS, 363, L66
Gunn J. E., Gott, III J. R., 1972, ApJ, 176, 1
Hahn O., Abel T., 2011, MNRAS, 415, 2101
Hahn O., Porciani C., Dekel A., Carollo C. M., 2009, MNRAS, 398, 1742
Hansen S. M., Sheldon E. S., Wechsler R. H., Koester B. P., 2009, ApJ, 699, 1333
Hartley W. G., Conselice C. J., Mortlock A., Foucaud S., Simpson C., 2015, MNRAS, 451, 1613
Hearin A. P., Watson D. F., 2013, MNRAS, 435, 1313
Hearin A. P., Watson D. F., Becker M. R., Reyes R., Berlind A. A., Zentner A. R., 2014a, MNRAS, 444, 729
Hearin A. P., Watson D. F., Becker M. R., Reyes R., Berlind A. A., Zentner A. R., 2014b, MNRAS, 444, 729
Hearin A. P., Watson D. F., Bosch F. C. v. d., 2015, MNRAS, 452, 1958
Hikage C., Mandelbaum R., Takada M., Spergel D. N., 2013, MNRAS, 435, 2345
Hinshaw G. et al., 2009, ApJS, 180, 225

Hirschmann M., De Lucia G., Wilman D., Weinmann S., Iovino A., Cucciati O., Zibetti S., Villalobos Á., 2014, MNRAS, 444, 2938

Hopkins P. F. et al., 2010, ApJ, 724, 915

Jing Y. P., Suto Y., Mo H. J., 2007, ApJ, 657, 664

Jose C., Srianand R., Subramanian K., 2014, MNRAS, 443, 3341

Kauffmann G. et al., 2003, MNRAS, 341, 33

Kauffmann G., Li C., Zhang W., Weinmann S., 2013, MNRAS, 430, 1447

Knobel C., Lilly S. J., Woo J., Kovač K., 2014, ArXiv e-prints: 1408.2553

Koester B. P. et al., 2007, ApJ, 660, 221

Kovač K. et al., 2014, MNRAS, 438, 717

Krause E., Hirata C. M., Martin C., Neill J. D., Wyder T. K., 2013, MNRAS, 428, 2548

Larson R. B., Tinsley B. M., Caldwell C. N., 1980, ApJ, 237, 692

Lu Y., Yang X., Shen S., 2015, ApJ, 804, 55

Ludlow A. D., Navarro J. F., Angulo R. E., Boylan-Kolchin M., Springel V., Frenk C., White S. D. M., 2014, MNRAS, 441, 378

Mao Y.-Y., Williamson M., Wechsler R. H., 2015, ApJ, 810, 21

Masaki S., Hikage C., Takada M., Spergel D. N., Sugiyama N., 2013a, MNRAS, 433, 3506

Masaki S., Lin Y.-T., Yoshida N., 2013b, MNRAS, 436, 2286

Moore B., Katz N., Lake G., Dressler A., Oemler A., 1996, Nature, 379, 613

More S., Miyatake H., Mandelbaum R., Takada M., Spergel D. N., Brownstein J. R., Schneider D. P., 2015, ApJ, 806, 2

More S., van den Bosch F. C., Cacciato M., Skibba R., Mo H. J., Yang X., 2011, MNRAS, 410, 210

Muldrew S. I. et al., 2012, MNRAS, 419, 2670

Navarro J. F., Frenk C. S., White S. D. M., 1996, ApJ, 462, 563

Navarro J. F., Frenk C. S., White S. D. M., 1997, ApJ, 490, 493

Oppenheimer B. D., Davé R., Kereš D., Fardal M., Katz N., Kollmeier J. A., Weinberg D. H., 2010, MNRAS, 406, 2325

Osmond J. P. F., Ponman T. J., 2004, MNRAS, 350, 1511

Paranjape A., 2014, Phys. Rev. D, 90, 023520

Peng Y.-j. et al., 2010, ApJ, 721, 193

Peng Y.-j., Lilly S. J., Renzini A., Carollo M., 2012, ApJ, 757, 4

Phillips J. I., Wheeler C., Boylan-Kolchin M., Bullock J. S., Cooper M. C., Tollerud E. J., 2014, MNRAS, 437, 1930

Prescott M. et al., 2011, MNRAS, 417, 1374

Rawlings S., Jarvis M. J., 2004, MNRAS, 355, L9

Ross A. J., Brunner R. J., 2009, MNRAS, 399, 878

Scoccimarro R., 1998, MNRAS, 299, 1097

Sheth R. K., Tormen G., 2004, MNRAS, 350, 1385

Skibba R., Sheth R. K., Connolly A. J., Scranton R., 2006, MNRAS, 369, 68

Skibba R. A., 2009, MNRAS, 392, 1467

Skibba R. A., Sheth R. K., 2009, MNRAS, 392, 1080

Skibba R. A., Sheth R. K., Croton D. J., Muldrew S. I., Abbas U., Pearce F. R., Shattow G. M., 2013, MNRAS, 429, 458

Skibba R. A., Sheth R. K., Martino M. C., 2007, MNRAS, 382, 1940

Skibba R. A. et al., 2014, ApJ, 784, 128

Skibba R. A., van den Bosch F. C., Yang X., More S., Mo H., Fontanot F., 2011, MNRAS, 410, 417

Somerville R. S., Davé R., 2014, ArXiv e-prints: 1412.2712

Springel V., 2005, MNRAS, 364, 1105

Tacchella S., Trenti M., Carollo C. M., 2013, ApJ, 768, L37

Tinker J. L., George M. R., Leauthaud A., Bundy K., Finoguenov A., Massey R., Rhodes J., Wechsler R. H., 2012, ApJ, 755, L5

Toomre A., Toomre J., 1972, ApJ, 178, 623

van den Bosch F. C., Aquino D., Yang X., Mo H. J., Pasquali A., McIntosh D. H., Weinmann S. M., Kang X., 2008, MNRAS, 387, 79

van den Bosch F. C., More S., Cacciato M., Mo H., Yang X., 2013, MNRAS, 430, 725

van der Wel A., Bell E. F., Holden B. P., Skibba R. A., Rix H.-W., 2010, ApJ, 714, 1779

Wang L., Weinmann S. M., De Lucia G., Yang X., 2013, MNRAS, 433, 515

Wang W., White S. D. M., 2012, MNRAS, 424, 2574

Watson D. F. et al., 2015, MNRAS, 446, 651

Wechsler R. H., Bullock J. S., Primack J. R., Kravtsov A. V., Dekel A., 2002, ApJ, 568, 52

Wechsler R. H., Zentner A. R., Bullock J. S., Kravtsov A. V., Allgood B., 2006, ApJ, 652, 71

Weinmann S. M., van den Bosch F. C., Yang X., Mo H. J., 2006, MNRAS, 366, 2

Wetzel A. R., Tinker J. L., Conroy C., 2012, MNRAS, 424, 232

Wetzel A. R., Tinker J. L., Conroy C., van den Bosch F. C., 2013, MNRAS, 432, 336

Wetzel A. R., White M., 2010, MNRAS, 403, 1072

White S. D. M., Rees M. J., 1978, MNRAS, 183, 341

Yang X., Mo H. J., van den Bosch F. C., Jing Y. P., 2005, MNRAS, 356, 1293

Yang X., Mo H. J., van den Bosch F. C., Pasquali A., Li C., Barden M., 2007, ApJ, 671, 153

York D. G. et al., 2000, AJ, 120, 1579

Zehavi I. et al., 2011, ApJ, 736, 59

Zehavi I. et al., 2005, ApJ, 630, 1

Zentner A. R., Hearin A. P., van den Bosch F. C., 2014, MNRAS, 443, 3044

Zhuravleva I. et al., 2014, Nature, 515, 85

APPENDIX A:

A1   The (in)dependence of galaxy red fractions on halo mass

As mentioned in the main text, one might expect in general that the distribution of galaxy colours depends on both galaxy luminosity and host halo mass. We explore this idea further in this Appendix.

Let the all-galaxy red fraction be some function $p(\mathrm{red}|M_r, m)$ at fixed galaxy luminosity and parent halo mass. Separating the red fractions of centrals and satellites, we can write this as

$$p(\mathrm{red}|M_r, m) = p(\mathrm{red}|\mathrm{cen}, M_r, m)\, p(\mathrm{cen}|M_r, m)$$
$$+ p(\mathrm{red}|\mathrm{sat}, M_r, m)\, p(\mathrm{sat}|M_r, m)\,, \quad (A1)$$

where $p(\mathrm{sat}|M_r, m)$ gives the fraction of galaxies that are satellites [so that $p(\mathrm{cen}|M_r, m) = 1 - p(\mathrm{sat}|M_r, m)$], and $p(\mathrm{red}|\mathrm{sat/cen}, M_r, m)$ gives the fraction of satellites/centrals

that are red. Any mass dependence in $p(\text{red}|\text{sat/cen}, M_r, m)$ could lead to "conformity-like" effects in analyses that average over halo mass (as we saw in Figure 5). What is usually referred to as conformity, however, is the statement that central and satellite colours are correlated even at *fixed* halo mass. Since we are trying to model the latter effect, it is important to understand the former as well.

For ease of notation, we define the following quantities that are fixed by the HOD:

$$\mathcal{N}_{\text{sat}}(< M_r|m) \equiv f_{\text{cen}}(< M_r|m)\bar{N}_{\text{sat}}(< M_r|m)$$
$$\mathcal{N}_{\text{sat}}(M_r|m) \equiv \partial\mathcal{N}_{\text{sat}}(< M_r|m)/\partial M_r$$
$$f_{\text{cen}}(M_r|m) \equiv \partial f_{\text{cen}}(< M_r|m)/\partial M_r \,, \qquad (A2)$$

where $f_{\text{cen}}(< M_r|m)$ and $\bar{N}_{\text{sat}}(< M_r|m)$ were introduced in section 2.1. The satellite fraction is then also fixed by the HOD as:

$$p(\text{sat}|M_r, m) = \frac{\mathcal{N}_{\text{sat}}(M_r|m)}{f_{\text{cen}}(M_r|m) + \mathcal{N}_{\text{sat}}(M_r|m)} \,, \qquad (A3)$$

In principle, however, we must calibrate the luminosity and mass-dependence of both $p(\text{red}|\text{sat}, M_r, m)$ and $p(\text{red}|\text{cen}, M_r, m)$. The S09 algorithm simplifies the problem by postulating that these two functions are approximately independent of parent halo mass. In other words, the S09 model states

$$p(\text{red}|M_r, m) = p(\text{red}|\text{cen}, M_r)\, p(\text{cen}|M_r, m)$$
$$+ p(\text{red}|\text{sat}, M_r)\, p(\text{sat}|M_r, m) \,, \quad (A4)$$

so that the all-galaxy red fraction still inherits a mass dependence from the HOD. S09 proceed to calibrate the function $p(\text{red}|\text{sat}, M_r)$ using clustering measurements of SDSS galaxies, and fix $p(\text{red}|\text{cen}, M_r)$ by demanding that the halo-averaged version of equation (A4) return the measured all-galaxy red fraction as a function of luminosity:

$$p(\text{red}|M_r) = p(\text{red}|\text{cen}, M_r)\, \bar{p}(\text{cen}|M_r)$$
$$+ p(\text{red}|\text{sat}, M_r)\, \bar{p}(\text{sat}|M_r) \,, \qquad (A5)$$

where

$$\bar{p}(\text{sat}|M_r) = \frac{\int \text{d}m\, n(m)\, \mathcal{N}_{\text{sat}}(M_r|m)}{\int \text{d}m\, n(m)\, [f_{\text{cen}}(M_r|m) + \mathcal{N}_{\text{sat}}(M_r|m)]} \,, \quad (A6)$$

and $\bar{p}(\text{cen}|M_r) = 1 - \bar{p}(\text{sat}|M_r)$, with $n(m)\text{d}m$ being the number density of m-halos.

The assumptions underlying equation (A4) were tested by Skibba (2009) by comparing colour distributions at fixed group richness as predicted by the S09 model with those in the Y07 and Berlind et al. (2006) catalogs. Overall the data appear consistent with the assumption that the red fractions at fixed M_r – of both satellites *and* centrals – do not depend on halo mass. As S09 point out, this may be expected for satellites, whose *luminosity* function is observed to be approximately halo mass-independent (Skibba et al. 2007; Hansen et al. 2009); the situation for the centrals, however, is less clear since their luminosity function does depend strongly on halo mass, at least for small masses. Also, the calibration by S09 using clustering measurements ignored effects of conformity and is therefore difficult to interpret in the present context. It is conceivable that a weak halo mass dependence $p(\text{red}|\text{cen}, M_r, m)$ might have litte consequence for the fixed-richness tests of Skibba (2009) but might have noticeable effects, e.g., in the red fraction profiles of Figures 5 and 6.

To assess the importance of such effects, we explore an alternative toy model which also assumes a mass-independent
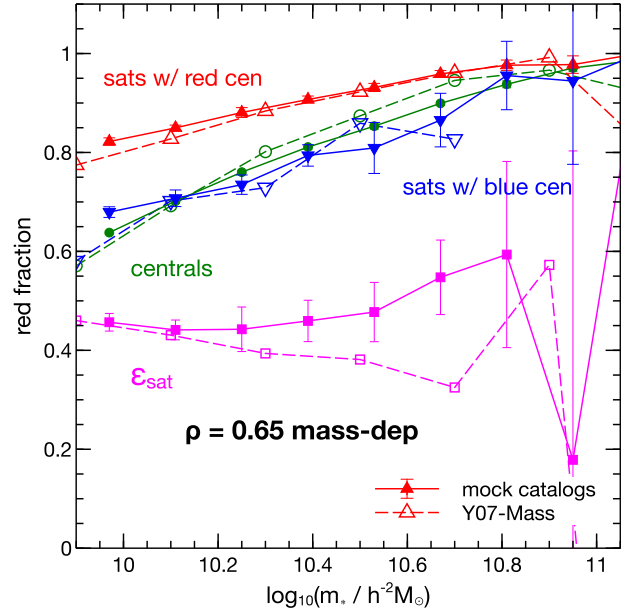
Figure A1. Comparison of the conformity-independent observables $f_{\text{red}|\text{cen}}$ (green circles) and ε_{sat} (magenta squares), and the conformity-dependent $f_{\text{red}|\text{sat},\text{rc}}$ (red triangles) and $f_{\text{red}|\text{sat},\text{bc}}$ (blue inverted triangles) in the Y07 catalog (open symbols with dashed lines) and in mocks that used $\rho = 0.65$ and a halo mass dependent central red fraction given by equations (A7)-(A9) (filled symbols with solid lines). The error bars on the mock results show the r.m.s. fluctuations around the mean value over 10 realisations.

satellite red fraction, but has a mass-*dependent* central red fraction $p(\text{red}|\text{cen}, M_r, m)$ whose average satisfies equation (A5), with $p(\text{red}|\text{sat}, M_r)$ and $p(\text{red}|M_r)$ given by equation (12) and the first of equations (9), respectively. At fixed luminosity, this model preferentially places red centrals in massive halos. In particular, denoting $\bar{p}_{\text{rc}} \equiv p(\text{red}|\text{cen}, M_r)$, we use

$$p(\text{red}|\text{cen}, M_r, m) = \bar{p}_{\text{rc}}\, \frac{g(M_r, m)}{\langle g(M_r, m) \rangle} \,, \qquad (A7)$$

where we set

$$g(M_r, m) = \bar{p}_{\text{rc}} + (1 - \bar{p}_{\text{rc}})\, \frac{\tanh(m/M_{\text{min}})}{\tanh(1)} \,, \qquad (A8)$$

with

$$\langle g(M_r, m) \rangle \equiv \frac{\int \text{d}m\, n(m)\, f_{\text{cen}}(M_r|m)\, g(M_r, m)}{\int \text{d}m\, n(m)\, f_{\text{cen}}(M_r|m)} \,, \qquad (A9)$$

and where $M_{\text{min}}(M_r)$ is the mass scale where $f_{\text{cen}}(< M_r|m) = 1/2$. The model is chosen such that in the limit of a step-like function $f_{\text{cen}}(< M_r|m) = \Theta(m - M_{\text{min}}(M_r))$, we would have $\langle g(M_r, m) \rangle = 1$ and $p(\text{red}|\text{cen}, m = M_{\text{min}}) = p(\text{red}|\text{cen}, M_r)$. The HOD we use has a smoother mass dependence in $f_{\text{cen}}(< M_r|m)$ and therefore our model requires a renormalisation by $\langle g(M_r, m) \rangle$. The model ensures $0 < p(\text{red}|\text{cen}, M_r, m) < 1$ in practice for all M_r and m.

Figure A1 shows the conformity-dependent satellite red fractions as well as the central red fraction and ε_{sat} when setting $\rho = 0.65$ in this model as the filled symbols joined by solid lines, formatted as in Figures 2 and 7. The open symbols with dashed lines again show corresponding measurements in the Y07-Mass catalog, and we see a good agreement between the mocks and the data. The 2-halo signal predicted by this
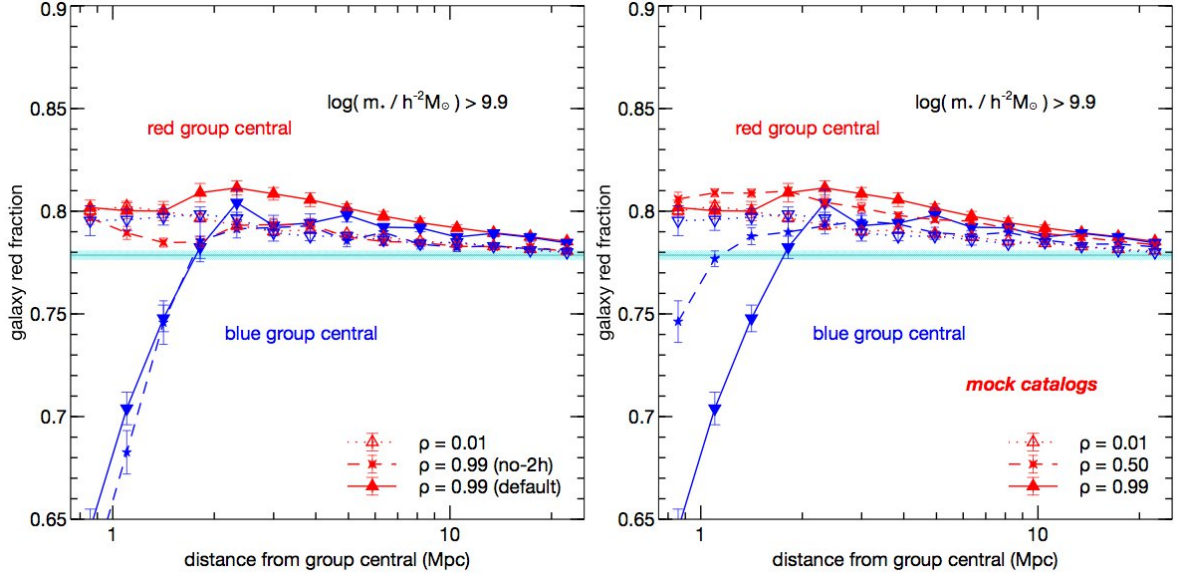
Figure A2. Same as the right panels of Figures 5 and 6 using the same set of mocks, except that the galaxy red fractions are measured centered on group centrals (centrals with at least one associated satellite) rather than isolated primaries. See text for a discussion.

model is shown in Figure 8 as the open symbols/dashed lines and is discussed in section 6.

A2   Large scale trends with and without conformity

Here we further explore the nature of large scale conformity in our mocks and argue that the trends seen in Figures 5 and 6 can be understood as a consequence of the relative bias of blue and red galaxies, together with the nature of halo assembly bias.

It is interesting to compare the results in the right panels of Figures 5 and 6 with similar measurements performed around "group centrals" rather than isolated primaries, where a group central is a central with at least one associated satellite. Firstly, we find that the number density of group centrals in our simulation box ($\sim 1.1 \times 10^{-3}(h/\mathrm{Mpc})^3$) is only about 16% that of isolated primaries, meaning that isolated primaries predominantly comprise of isolated *singletons* which occupy low mass halos, which is not surprising considering that $\sim 90\%$ of all centrals are singletons. The all-galaxy red fraction surrounding group centrals is shown in Figure A2, whose left and right panels are formatted exactly like the right panels of Figures 5 and 6, respectively. We see, e.g., that the magnitude of the difference between the $\rho = 0.99$ red fractions around red and blue group centrals is substantially reduced as compared to that around isolated primaries. At scales larger than $\sim 15\mathrm{Mpc}$, the *no-2h* mocks show red fractions consistent with the global average, while the default mocks with increasingly larger ρ show correspondingly larger red fractions.

To understand these trends, consider the simpler measurement of the galaxy red fraction at a distance r from an *arbitrary* red central, $f_{\mathrm{red}|\mathrm{rc}}(r)$. A straightforward calculation shows that we can write this as

$$f_{\mathrm{red}|\mathrm{rc}}(r) = \left(1 + \left(\frac{\bar{n}_{\mathrm{b}}(1 + \xi_{\mathrm{b,rc}}(r))}{\bar{n}_{\mathrm{r}}(1 + \xi_{\mathrm{r,rc}}(r))} \right) \right)^{-1}, \qquad (A10)$$

where $\bar{n}_{\mathrm{b(r)}}$ is the mean number density of blue (red) galaxies and $\xi_{\mathrm{b(r),rc}}(r)$ is the cross-correlation function between blue (red) galaxies and red centrals. A similar expression holds for

the red fraction around blue centrals $f_{\mathrm{red}|\mathrm{bc}}(r)$, with the replacement 'rc'→'bc' in the correlation functions on the r.h.s. of equation (A10).

The correlation functions above can be split into contributions arising from galaxies in the same halo as the central object or in different halos (the 1-halo and 2-halo terms, respectively): $\xi(r) = \xi^{(1\mathrm{h})}(r) + \xi^{(2\mathrm{h})}(r)$. Recall that 1-halo terms dominate at small separations and 2-halo terms at large separations. For sufficiently large separations the 2-halo terms also become small compared to unity. We now observe the following:

- **Red fraction profile:**
At scales large enough that the 2-halo contributions dominate but are not yet negligible compared to unity, $f_{\mathrm{red}|\mathrm{rc}}(r)$ will have an r-dependence given by replacing $\xi(r) \to \xi^{(2\mathrm{h})}(r)$ in equation (A10). In general, the correlation functions would not conspire to precisely cancel the r-dependence in this regime. Therefore, only when *both* 2-halo correlations have become substantially smaller than unity will the asymptotic value $f_{\mathrm{red}|\mathrm{rc}}(r) \to (1 + \bar{n}_{\mathrm{b}}/\bar{n}_{\mathrm{r}})^{-1} = \bar{f}_{\mathrm{red}}$ be reached. To get a rough estimate of when this will occur, let us ignore complications introduced by mass completeness, colour cuts, etc. and simply use a power law fit for the all-galaxy correlation function of our luminosity complete sample: $\xi(r) \sim (r/7\mathrm{Mpc})^{-1.85}$ (Zehavi et al. 2011). It is therefore not surprising that all our data sets, including the ones with $\rho = 0.01$, show significant red fraction profiles at distances less than $\sim 15\mathrm{Mpc}$.
- $f_{\mathrm{red}|\mathrm{rc}}(r) = f_{\mathrm{red}|\mathrm{bc}}(r)$ **at large r for all models:**
At large separations, it is reasonable to assume that halo bias is approximately linear and scale-independent. The 2-halo cross-correlations above can then be written as Fourier transforms of cross-power spectra that take the form $P^{(2\mathrm{h})}_{\mathrm{b(r),rc}}(k) = P_{\mathrm{lin}}(k)\, \bar{b}_{\mathrm{rc}}\, \bar{b}_{\mathrm{b(r)}}(k)$ for $\xi^{(2\mathrm{h})}_{\mathrm{b(r),rc}}(r)$, where $\bar{b}_{\mathrm{b(r)}}(k)$ is the number-weighted halo bias associated with all blue (red) galaxies while $\bar{b}_{\mathrm{rc}}$ is the corresponding term for red centrals alone, and $P_{\mathrm{lin}}(k)$ is the dark matter power spectrum in linear theory (see, e.g., Cooray & Sheth 2002). (The scale dependence in the all-galaxy bias arises from the profiles of satellites within a halo, while
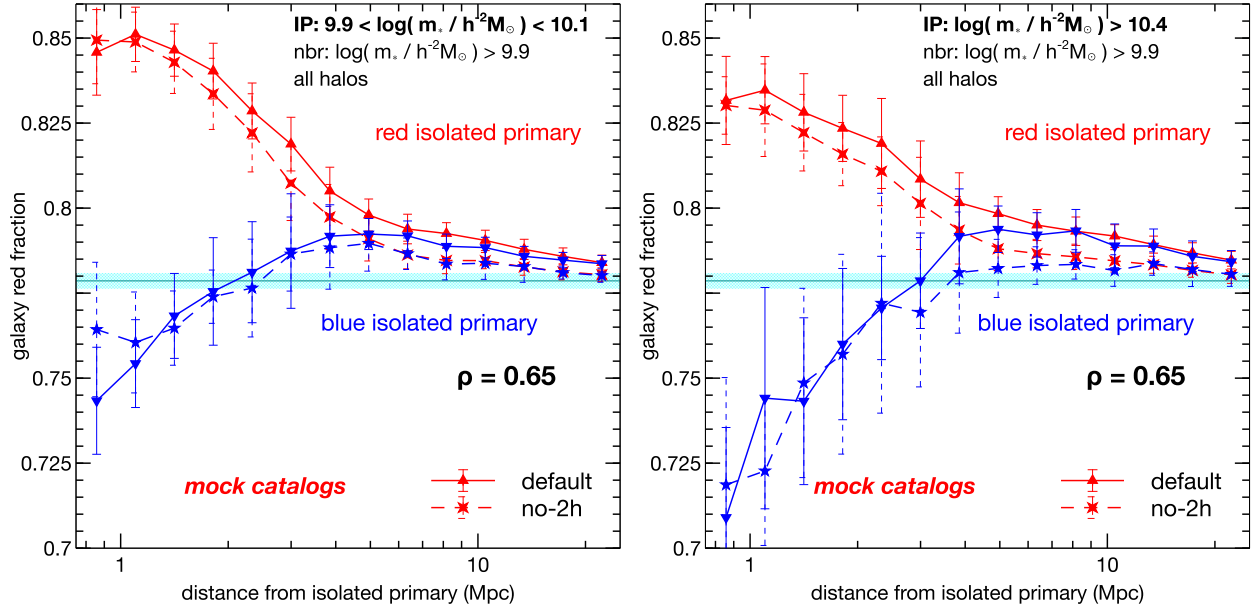
Figure A3. Same as Figure 8, showing the large scale conformity signal for the default and *no-2h* mocks around isolated primaries with $9.9 < \log_{10}(m_\star) < 10.1$ *(left panel)* and $\log_{10}(m_\star) > 10.4$ *(right panel)*.

the central-only term has no such scale dependence.) In the regime where both these terms are larger than unity, the scale independent $\bar{b}_{\rm rc}$ cancels in their ratio. A similar factor $\bar{b}_{\rm bc}$ cancels when constructing $f_{\rm red|bc}(r)$ as well, which means that we will have $f_{\rm red|rc}(r) \approx f_{\rm red|bc}(r)$ in this regime for any value of ρ. Indeed, we see this behaviour at large scales in Figure A2.

• **All red fractions are larger than $\bar{f}_{\rm red}$:**
The red fractions (even in the absence of 2-halo conformity) approach the global mean from *above* rather than below because the average bias factors of blue and red galaxies satisfy $\bar{b}_{\rm b} < \bar{b}_{\rm r}$. This may seem counter-intuitive since, on average, blue galaxies in a mass-complete sample are more luminous and therefore preferentially occupy more massive halos than red galaxies. However, the halo mass distribution of red galaxies is substantially broader than that of blue galaxies, with a longer tail at high masses that pushes the number-weighted red galaxy bias $\bar{b}_{\rm r}$ to be larger than $\bar{b}_{\rm b}$. In the luminosity complete sample, this effect is further enhanced due to the inclusion of a large number of faint blue objects (predominantly centrals) which also live in low mass halos.

• **Increase of 2-halo conformity red fractions with ρ:**
The reason that the red fractions in the presence of 2-halo conformity increase with ρ is the presence of halo assembly bias at large scales. In this case the bias factors above contain integrals of the form $\sim \int d \ln m \int ds\, p(s|m)\, b(m,s)\, \Phi_{\rm blue(red)}(m,s)$ which couple the concentration-dependence of halo bias to that of the red fraction in our model. The number weighting of bias means that small mass halos ($m_{\rm 200b} \sim 10^{11.8} h^{-1} M_\odot \sim 0.25 M_*$) will dominate the integral. If the bias $b(m,s)$ for such halos were monotonically increasing with s, then a straightforward calculation shows that a large positive value of ρ would enhance the difference between $\bar{b}_{\rm b}$ and $\bar{b}_{\rm r}$ discussed previously, consequently increasing the red fractions. Although the actual behaviour of the bias for masses $\sim 0.25 M_*$ is non-monotonic and shows a minimum around $s = 0$ (see, e.g., Figure 4 of Wechsler et al. 2006), the fact that the majority of galaxies in the mass-complete sample are red for any halo mass means that this trend does not change. Interestingly, the amplitude

of this signal appears stable against a possible weak mass dependence in the central red fraction (see Figure 8), suggesting that an enhanced value of $f_{\rm red|rc}(r) \simeq f_{\rm red|bc}(r)$ at $r \gtrsim 8\text{Mpc}$ as compared to the global average could be a robust indicator of 2-halo conformity.

• $f_{\rm red|rc}(r) > f_{\rm red|bc}(r)$ **for** $r \lesssim 5\text{Mpc}$ **for** $\rho = 0.99$ **with 2-halo conformity:**
For $\rho = 0.99$, the term "red fraction" is essentially the same as "fraction with large halo concentration s" (equation 3). When computing red fractions we are then actually asking: what is the fraction of large-s objects around (a) large-s objects and (b) small-s objects? If we now focus on separations $r \lesssim 5\text{Mpc}$, we are directly studying a version of halo assembly bias in a range of scales (the so-called "1-halo to 2-halo transition" regime) where the previous assumptions regarding linear scale-independent biasing are no longer valid.

Consider centrals in low mass halos first (e.g., the isolated singletons from earlier). Due to assembly bias, the ones with large s will cluster strongly with other large-s centrals of similar halo mass, while the small-s centrals will be close to unbiased. The number weighting will ensure that this behaviour gives the dominant effect in the vicinity of small halo centrals, with little contribution from satellites and centrals in more massive halos. This will lead to a large difference in $f_{\rm red|rc}(r)$ and $f_{\rm red|bc}(r)$ at small distances, which must then smoothly match the large scale trend of $f_{\rm red|rc}(r) \approx f_{\rm red|bc}(r)$, consistent with what is seen in Figures 5 and 6.

Group centrals that reside in more massive halos are likely to have other high mass halos nearby due to larger average halo bias, so that assembly bias will still be active. However, contamination due to nearby singletons (which reside in less clustered, lower mass halos) and the fact that assembly bias reverses its trend around the global characteristic halo mass will mean that the strength of the difference in red fractions will be smaller here. This is consistent with the results in Figure A2.

• $\rho = 0.99$ **without 2-halo conformity:**
For the model with $\rho = 0.99$ and 2-halo conformity switched
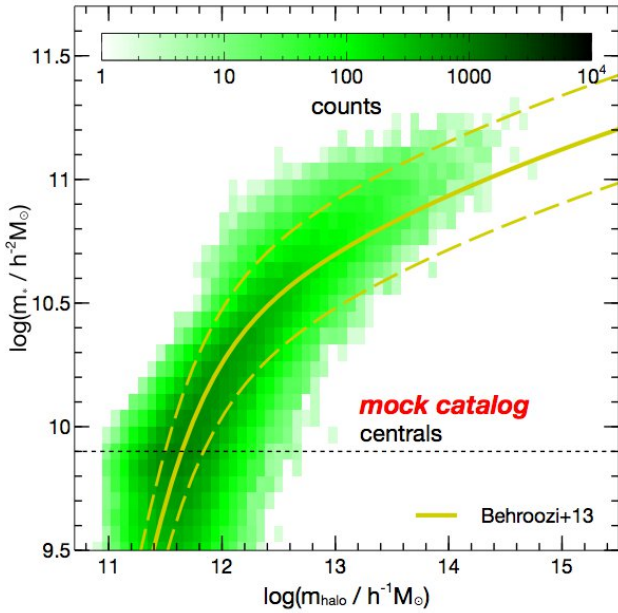
Figure A4. Joint distribution of stellar mass of centrals and their parent halo mass. For comparison, the smooth yellow curves show the median stellar mass at fixed halo mass (solid curve) and its 1-sigma scatter (dashed curves) as calibrated by Behroozi et al. (2013a) at redshift $z = 0$. The horizontal dotted line shows our mass completeness limit at $\log_{10}(m_\star) = 9.9$.

off, we expect that at large scales $f_{\mathrm{red|rc}} = f_{\mathrm{red|bc}}$ while at small scales $f_{\mathrm{red|rc}} \to 1$ and $f_{\mathrm{red|bc}} \to 0$. The transition between these extremes will be dramatic but smooth due to averaging over halo mass, and should occur in the same "1-halo to 2-halo transition" regime discussed above. This is consistent with what we see in the right panel of Figure 5, where the transition occurs around $r \sim 3\text{-}4\mathrm{Mpc}$. In the left panel of Figure A2 we essentially see only the large scale behaviour; presumably this is because we do not impose any isolation criterion in the group central measurement and therefore end up selecting very small groups (of which there are many). The isolation criterion in Figure 5 on the other hand would select relatively large groups (in addition to the very high number of singletons which would however not contribute any 1-halo signal). This effect adds to *and confuses* the transition regime 2-halo conformity effect discussed above, particularly when studying projected signals. We discuss this further in section 6.

Finally, the two panels of Figure A3 are formatted identically to Figure 8 and show that the large scale conformity signal in our mocks is essentially independent of the stellar mass of the isolated primary, an effect we attribute to the large scatter in the distribution of halo masses at fixed stellar mass as seen in Figure A4.